Deformation of western Turkey from a combination of permanent and campaign GPS data: Limits to block-like behavior

B. Aktug, J.-M. Nocquet, A. Cingöz, B. Parsons, Y. Erkan, P. England, O. Lenk, M.-A. Gürdal, A. Kilicoglu, H. Akdeniz, et al.

▶ **To cite this version:**

B. Aktug, J.-M. Nocquet, A. Cingöz, B. Parsons, Y. Erkan, et al.. Deformation of western Turkey from a combination of permanent and campaign GPS data: Limits to block-like behavior. Journal of Geophysical Research, 2009, 114, pp.B10404. 10.1029/2008JB006000 . hal-00460769

HAL Id: hal-00460769
https://hal.science/hal-00460769

Submitted on 10 Sep 2021

HAL is a multi-disciplinary open access archive for the deposit and dissemination of scientific research documents, whether they are published or not. The documents may come from teaching and research institutions in France or abroad, or from public or private research centers.

L'archive ouverte pluridisciplinaire **HAL**, est destinée au dépôt et à la diffusion de documents scientifiques de niveau recherche, publiés ou non, émanant des établissements d'enseignement et de recherche français ou étrangers, des laboratoires publics ou privés.

Copyright

Deformation of western Turkey from a combination of permanent and campaign GPS data: Limits to block-like behavior

B. Aktug,[1] J. M. Nocquet,[2,3] A. Cingöz,[1] B. Parsons,[2] Y. Erkan,[1] P. England,[2] O. Lenk,[1] M. A. Gürdal,[1] A. Kilicoglu,[1] H. Akdeniz,[1] and A. Tekgül[1]

Received 9 August 2008; revised 10 June 2009; accepted 13 July 2009; published 22 October 2009.

[1] We present a new geodetic velocity field covering western Turkey, south of the North Anatolian fault. Our velocity field is derived from a combination of continuously recording GPS stations operating since 2003, survey-type GPS measurements carried out in the period 1997–2005, and velocities from Reilinger et al. (2006). The velocity field indicates that western Turkey currently undergoes extension whose rate increases from the Anatolia plateau to the Aegean coast. The overall extension in westernmost Turkey is about 20 mm/yr, making it one of the fastest areas of continental extension in the world. We test whether the observed deformation is better represented by the rotation of crustal blocks or by more distributed deformation. While no deformation is detected in the central Anatolian plateau, we observe a deformation field west of the plateau that cannot be explained by block models, unless the blocks are so small as to be essentially indistinguishable from a continuum. Although concentration of strain rates (up to 140 nstrain/yr) are found across the major grabens, strain rates above 50 nstrain/yr are found throughout western Turkey. The distributions of topography and crustal thickness in western Turkey agree with the distributions expected if the crust there had a constant thickness at 5 Ma, equal to that of the present central Anatolian plateau, and had subsequently been thinned at the present-day distribution of strain rates. Our results, therefore, suggest that extensional strain affects the whole continental lithosphere of western Turkey, rather than being restricted to a small number of block boundaries.

Citation: Aktug, B., et al. (2009), Deformation of western Turkey from a combination of permanent and campaign GPS data: Limits to block-like behavior, *J. Geophys. Res.*, *114*, B10404, doi:10.1029/2008JB006000.

1. Introduction

[2] How continents deform is still a matter of debate. The essential questions concern what are the most appropriate descriptions of the deformation, of the rheology of the continental lithosphere, and of the forces driving the deformation. One viewpoint is that zones of continental deformation are composed of a limited number of rigid or elastic microplates or crustal blocks [*Nyst and Thatcher*, 2004; *Reilinger et al.*, 2006]. If this is so, the surface motion can then be appropriately described by the relative rotation of the blocks, and strain will be localized along, or close to, the major faults separating the blocks. A contrasting viewpoint is that deformation at depth is distributed throughout the continental lithosphere, with the motion of the upper crust simply reflecting the deeper deformation so that faults in the upper crust are not required to extend to great depths. Global Positioning System (GPS) measurements, by measuring the present-day surface deformation at the millimeter-per-year level in a consistent reference frame, have the potential to determine which kinematic description of continental deformation best fits the observed deformation.

[3] Turkey is often considered to provide some of the best evidence for the rigid block description of continental deformation [e.g., *McClusky et al.*, 2000]. The North Anatolian fault, slipping at ~25 mm/yr, defines a major boundary separating the motion of Anatolia from Eurasia, with slow deformation in the rest of central Turkey (<2mm/yr [*McClusky et al.*, 2000]). In western Turkey, south of the North Anatolian fault and west of longitude ~30°E, the distribution of earthquakes indicates that the crust is undergoing active deformation (Figure 1). Large active grabens and thinned crust [*Saunders et al.*, 1998; *Sodoudi et al.*, 2006] indicate significant stretching of the crust in a roughly north-south direction. Recent studies by *Nyst and Thatcher* [2004] and *Reilinger et al.* [2006] concluded that a small number (3–4) of rigid blocks could account for GPS determinations of velocity in western Turkey. Each study, however, noticed departures from rigid behavior; *Nyst and Thatcher* [2004] found extensional strain rates of 40 to 50 nstrain/yr within their Anatolia, South Aegean and South Marmara blocks, and *Reilinger et al.* [2006] noticed large residual motions (~7 mm/yr) induced by extensional deformation unmodeled by the block approach.

[1] General Command of Mapping, Ankara, Turkey.
[2] COMET, Department of Earth Sciences, Oxford, UK.
[3] CNRS-Geosciences Azur, University of Nice-Sophia-Antipolis, Valbonne, France.

Copyright 2009 by the American Geophysical Union.
0148-0227/09/2008JB006000$09.00

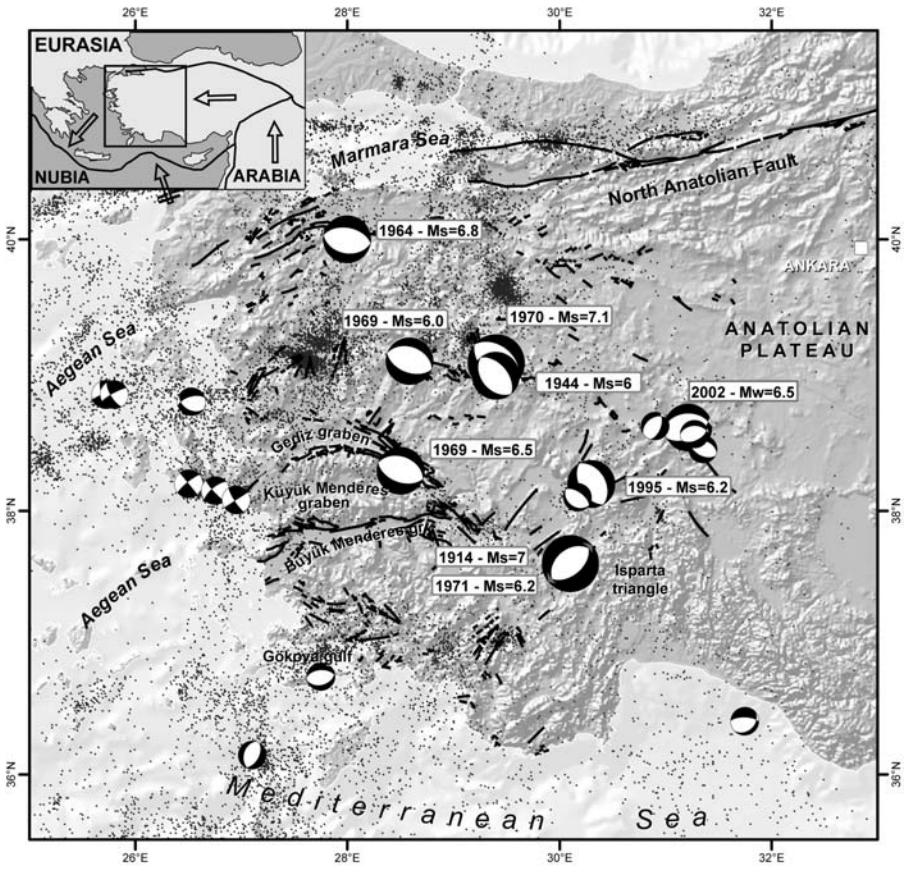

Figure 1. Seismicity and active faults in western Turkey. Dots show epicenters from the National Earthquake Information Center (NEIC) for the period 1976–2006. Labeled focal mechanisms represent earthquakes with $M_s \geq 6$ taken from *Ambraseys and Jackson* [1998], except the 1969 Demirci $M_s = 6.0$ earthquake from *Eyidogan and Jackson* [1985] and the 2002 M_w 6.5 Sultandagi earthquake from the Global CMT catalogue. Other, unlabeled, focal mechanism are taken from the Global CMT catalogue (http://www.globalcmt.org) for crustal earthquakes with $M_w \geq 5$. Faults are from *Saroglu et al.* [1992].

[4] In this study, we present a velocity field that includes more than 120 sites covering central Anatolia to the Aegean coast, with an average intersite distance of ~50 km, determined at a millimeter-per-year accuracy. Our velocity field is derived from a combination of survey-type GPS (SGPS), spanning the period 1997–2005 and a network of 12 continuously recording GPS stations (CGPS) operating at 7 sites since 2003 and for a further 5 sites since 2005. CGPS provides unique data sets for rigorously assessing crustal deformation in regions of low strain rates by reducing the amount of time necessary to detect a significant strain signal, minimizing systematic errors, and providing a rigorous assessment of uncertainties through the quantification of the noise present in the coordinate time series. However, the high cost of installation and maintenance of CGPS stations and the need for good security conditions at the sites limit the number of sites. In contrast, SGPS allows a larger number of sites but can be easily affected by systematic errors, such as those due to tribrach miscalibration or centering problems. An optimum velocity field can be obtained by a combination of the two types of data, and we present here a methodology that enables us to do this rigorously. We then use the resulting geodetic velocity field to quantify the level of deformation of the Anatolian plateau and to determine the location of the onset of the extension. We test it against previously published models and discuss the ability of rigid block models to account for the observed deformation in western Turkey.

2. Data Set

2.1. Data Set Description

[5] The survey-type GPS measurements were made at 69 sites during at least two of the five surveys carried out between 1997 and 2005 (Table 1). Each GPS site was observed during at least two sessions of 7 h in each survey. The COMET-GCM CGPS network includes 12 sites across western Turkey from the central Anatolian plateau (longitude 32°E) to the Aegean coast and south of the North Anatolian fault. Each site consists of a 1-m-high concrete circular pillar, thermally isolated by a concrete tube surrounding the pillar. Each pillar is anchored to the bedrock through steel rods penetrating the rock by over 50 cm. A Trimble 5700 dual-frequency GPS receiver with a Trimble Zephyr Geodetic antenna is operated at all sites except KNYA (Konya), which is equipped with a Trimble SSI receiver with a Trimble Choke-Ring antenna. A Trimble hemispheric radome covers the antenna at sites where snow is abundant during the winter. Seven sites were installed in 2003 and benefit from at least 3 years of data

Table 1. Observation Spans of the Survey Sites Processed in This Study[a]

Site	λ[b]	φ[b]	Start[c]	End[c]	Span[c]	q	2000	2001	2003	2005
afyo	30.644	38.769	1997.86	2005.34	7.47	x	x	x		x
AKHI	**28.010**	**38.960**	**2003.49**	**2006.83**	**3.34**					**x**
aksh	31.481	38.342	1997.86	2005.34	7.47	x		x		x
aksu	31.121	37.762	1997.83	2000.79	2.96	x			x	
alan	27.425	39.785	1997.77	2005.34	7.57	x	x			x
ANKR	**32.759**	**39.887**	**1997.62**	**2005.34**	**7.72**	**x**	**x**	**x**		**x**
ayag	32.812	39.660	1997.70	2005.34	7.63	x				x
ayka	26.700	39.311	1997.77	2005.34	7.57	x	x			x
bahr	50.608	26.209	1997.62	2005.34	7.72	x	x	x	x	x
bayo	27.308	38.711	1997.79	2005.34	7.55	x	x			x
bder	26.190	39.614	1997.77	2005.34	7.57	x	x			x
BCAK	**30.720**	**37.320**	**2005.37**	**2006.83**	**1.45**					**x**
bhtl	30.589	36.896	1997.83	2005.34	7.51	x				x
bltp	29.786	39.566	1997.71	2005.34	7.63	x	x			x
bost	27.099	38.453	1997.79	2005.34	7.55	x				x
BOZU	**30.049**	**39.881**	**2003.97**	**2006.83**	**2.86**					**x**
buck	30.579	37.446	1997.83	2005.34	7.51	x				x
byda	28.227	38.067	1997.79	2005.34	7.55	x				x
bysh	31.658	37.656	1997.86	2000.79	2.93	x			x	
bzkr	29.609	37.803	1997.83	2000.79	2.96	x			x	
ceil	26.385	38.311	1997.79	2000.73	2.94	x	x			
cift	29.096	36.691	1997.83	2005.34	7.51	x				x
CINC	**27.960**	**37.63**	**2005.36**	**2006.83**	**1.46**					**x**
cine	28.081	37.609	1997.79	2005.34	7.55	x				x
cmlk	27.380	37.878	1997.79	2005.34	7.55	x				x
dlmn	28.826	36.762	1997.79	2000.79	3.00	x			x	
dmir	28.671	39.046	1997.77	2000.73	2.96	x	x			
durs	28.635	39.611	1997.77	2005.34	7.57	x	x			x
elmi	29.810	36.790	2005.37	2006.83	1.45					
emet	29.246	39.335	1997.86	2005.34	7.47	x	x			x
erde	27.808	40.393	2001.78	2005.34	3.56			x		x
ESME	**28.994**	**38.505**	**2003.48**	**2006.34**	**3.35**					**x**
gbiz	30.948	37.115	1997.83	2000.79	2.96	x			x	
gkpn	29.392	37.448	1997.83	2000.79	2.96	x			x	
hoba	26.535	39.580	1997.77	2000.73	2.96	x	x			
hrdl	28.822	38.339	1997.79	2005.34	7.55	x				x
huyk	31.571	37.898	1997.86	2005.34	7.47	x				x
isrt	30.592	37.820	1997.83	2000.79	2.96	x			x	
ista	29.019	41.104	2000.73	2005.34	4.61		x	x		x
keme	30.548	36.552	1997.83	2005.34	7.51	x				x
KIT3	**66.885**	**39.135**	**1997.62**	**2005.34**	**7.72**	**x**	**x**	**x**	**x**	**x**
kmlc	30.272	36.370	1997.83	2000.79	2.96	x			x	
KNYA	**32.505**	**38.022**	**2003.70**	**2006.83**	**3.13**					**x**
koca	29.045	38.731	1997.86	2005.34	7.47	x	x			x
kony	32.394	37.869	1997.86	1997.86	0.00	x				
krct	30.617	39.260	1997.86	2005.34	7.47	x				x
krku	30.178	37.043	1997.83	2005.34	7.51	x				x
kula	28.740	38.574	1997.79	2005.34	7.55	x				x
kybl	29.263	36.423	1997.83	2005.34	7.51	x				x
kybs	29.810	36.971	1997.83	2000.79	2.96	x			x	
mese	32.577	39.869	1997.70	2000.73	3.02	x	x			
mhmt	30.546	38.501	1997.86	2005.34	7.47	x		x		x
MIHA	**31.457**	**39.847**	**2003.35**	**2006.83**	**3.52**					**x**
MNTS	**26.717**	**38.427**	**2003.70**	**2006.83**	**3.13**					**x**
mula	28.427	37.175	1997.79	2000.79	3.00	x			x	
NICO	**33.396**	**35.141**	**1997.70**	**2006.83**	**9.13**	**x**	**x**	**x**	**x**	
sima	29.042	39.147	1997.86	2000.73	2.86	x	x			
slck	32.506	38.022	1997.71	1997.86	0.15	x				
sllr	29.554	38.150	1997.83	2005.34	7.51	x				x
srkk	31.228	38.163	1997.86	2005.34	7.47	x		x	x	x
sryn	32.471	38.237	1997.86	2005.34	7.47	x				x
stcl	31.001	37.475	1997.83	2000.79	2.96	x			x	
suba	26.174	39.973	1997.77	2000.73	2.96	x	x			
tava	29.048	37.566	1997.83	2000.79	2.96	x			x	
TVAS	**29.140**	**37.410**	**2005.37**	**2006.83**	**1.45**					**x**
thrn	28.584	37.576	1997.79	2005.34	7.55	x				x
tkin	30.114	38.016	1997.83	2005.34	7.51	x				x
tprk	30.631	38.105	1997.83	2000.79	2.96	x			x	
TRAB	**39.776**	**40.995**	**2000.73**	**2006.83**	**6.10**		**x**	**x**		**x**
trmn	30.387	39.431	1997.86	2000.73	2.86	x	x			
TUBI	**29.451**	**40.787**	**2000.73**	**2006.83**	**6.10**		**x**	**x**		**x**
uctp	27.613	38.263	1997.79	2005.34	7.55	x				x
ugur	30.503	37.316	1997.83	2000.79	2.96	x			x	

Table 1. (continued)

Site	λ^b	φ^b	Start[c]	End[c]	Span[c]	q	2000	2001	2003	2005
ulub	29.240	38.417	1997.86	2005.34	7.47	x				x
ULUT	**29.131**	**40.098**	**2000.73**	**2006.83**	**6.10**		**x**		**x**	**x**
uris	26.742	38.384	1997.79	2005.34	7.55	x				x
yeme	32.240	39.099	1997.86	2005.34	7.47	x	x			x
yenf	26.791	38.741	1997.79	2000.73	2.94	x	x			
ykcf	29.922	36.658	1997.83	2005.34	7.51	x				x
ynak	31.706	38.831	1997.86	2005.34	7.47	x		x		x
ysfc	29.535	37.185	1997.83	2000.79	2.96	x			x	
YUNA	**31.730**	**38.802**	**2003.96**	**2006.83**	**2.87**					**x**

[a]CGPS sites are indicated by bold letters; 1997–2005 are the years of the GPS surveys.
[b]Longitude and latitude in decimal degrees.
[c]Start, end, and observation time span in decimal years.

in our solution (Table 1). Five sites installed in 2005 have a data span of about 1.5 years in our solution.

2.2. Data Analysis

[6] Survey data were processed at the General Command of Mapping of Turkey (GCM), using the Bernese v5.0 software [*Rothacher and Mervart*, 1996] while CGPS data were processed at COMET using the GAMIT software (release 10.3 [*King and Bock*, 2006]). Each set of processing uses a standard strategy for geodynamics. Beside our network in western Turkey, we include 14 IGS sites surrounding western Turkey and six IGS sites located in Turkey and Cyprus (TRAB, MERS, ANKR, ISTA, TUBI, NICO). Two sites for which data are archived at UNAVCO (LAUG, CRAO) were also included in our processing. These IGS sites are used to define the reference frame and to tie the CGPS solution to other solutions at the combination step. We also include the continuous GPS station at ULUT from the MAGNET network [*Ergintav et al.*, 2002] to augment our network in western Turkey. The processing of both data set uses IGS final orbits, absolute elevation-dependent antenna phase center models following the tables recommended by the IGS, solid Earth and polar tide corrections following the 2003 IERS conventions [*McCarthy and Petit*, 2004], and ocean tide loading corrections using the CSR4.0 ocean tide model [*Eanes and Schuler*, 1999]. As a result of the processing, we produce loosely constrained solutions including the estimated coordinates with the associated full covariance matrix.

2.3. Time Series Analysis

[7] The generation of time series is not a direct step in our analysis, but rather is carried out in parallel to get the proper weighting for the velocity uncertainties of the CGPS solution. Time series are obtained by expressing our daily solutions in the International Terrestrial Reference Frame (ITRF) ITRF2005 [*Altamimi et al.*, 2007] using a seven-parameter transformation. Long-term repeatabilities are 2 mm in the horizontal components and 6 mm for the vertical component. At this step, we examine all of the coordinate time series for outliers and jumps. Most of our time series (Figure 2) for western Turkey show an annual signal superimposed on a long-term trend. Such signals reflect the unmodeled elastic response of the solid Earth induced by mass redistribution in the atmosphere, the oceans and continental [*Van Dam et al.*, 2001; *Dong et al.*, 2002], possible mismodeling of the seasonal variations in the tropospheric delays, and possible reference frame effects. All sites in western Turkey show a statistically significant annual component, with magnitude of 1–2 and 0.5 mm in the north and east components, respectively. For these sites, the time series are consistent in phase with a maximum during the winter for the north component and a maximum in the summer for the east component. The semiannual component is usually insignificant (<0.7 mm).

[8] *Blewitt and Lavalle* [2002] showed that periodic seasonal signals affect velocity estimates, particularly when the data span available is short (i.e.,<2.5 years). In order to assess the impact of such signals on our velocity estimates for sites having between 1.5 and 2.0 years of data, we compared, for sites having at least 3 years of data, the velocity estimated for 1.5–2.0 years with its value derived from the full time series. The maximum discrepancy found is 1.3 mm/yr and is similar to the standard deviation found for this length of time series. We therefore kept the sites with only 1.5–2.0 years of data in order to improve the redundancy when combining the CGPS solution with the GPS survey solutions.

[9] We used the maximum likelihood estimator (MLE) procedure embedded in the CATS software [*Williams*, 2003] to best describe the noise characteristics of our time series and obtain realistic uncertainties on velocity estimates. We found that a combination of white and flicker noise best explains the noise content of the time series, as is the case for most CGPS solutions [*Williams et al.*, 2004]. Only 3% (north component), 0% (east component), 10% (up component) of the time series showed a preferred noise model including white noise and random walk noise. As a consequence of the presence of colored noise in the time series, the standard deviation of the horizontal velocity components obtained using a correct noise model are on average 6.4 (north) and 5.8 (east) times larger than those derived assuming white noise only. The Kalman filter implemented in the GLOBK software [*Herring et al.*, 1990, 2006] can account for time-correlated noises through Gauss-Markov processes. We used an empirical approach, calibrating the values of the Gauss-Markov noise for each component of each site in such a way that GLOBK provides a standard deviation in velocity similar to the ones obtained by the MLE algorithm. Applying this approach, we find typical standard deviations (1 σ) in the horizontal velocity com-

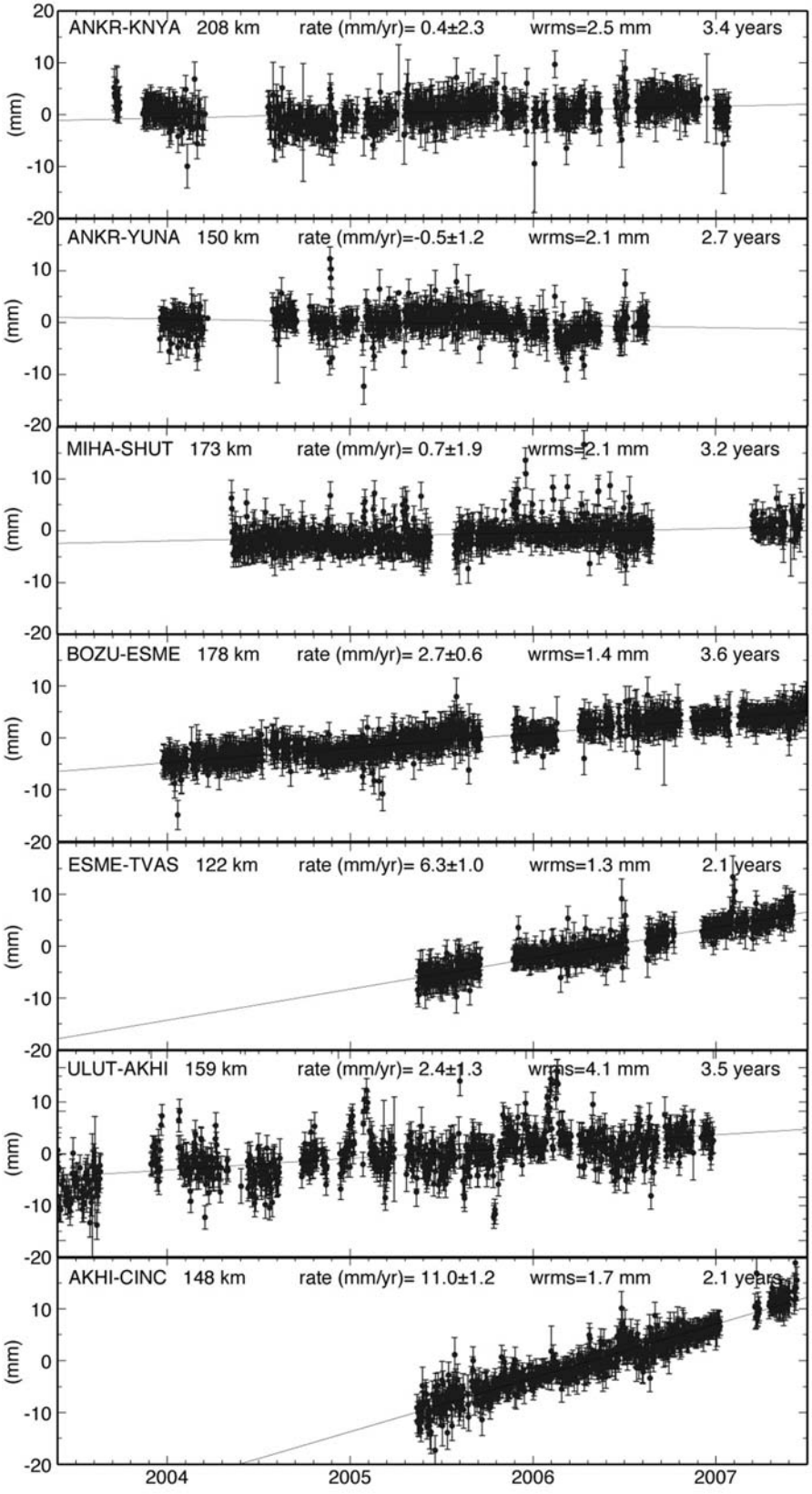

Figure 2. Time series for pairs of CGPS sites that illuminate particular aspects of the velocity field (see section 4.2.1). See Figure 3 for the location of the CGPS sites and baselines. Rate uncertainties are at the 95% confidence level and are obtained including a combination of white and flicker noise using the method described by *Williams* [2003].

ponents of 0.5 mm/yr for sites having 3.5 years of data, and 1.0 mm/yr for sites having 1.5 years of data.

3. A Combination Solution

[10] A rigorous combination of various types of geodetic data does not necessarily require that the original observations are analyzed simultaneously, provided that the full variance-covariance matrices and the full description of constraints applied to individual solutions are available and can be removed [*Brockmann*, 1996; *Dong et al.*, 1998; *Altamimi et al.*, 2002]. In the combination approach, the observations are first reduced to a set of parameters of interest (e.g., the coordinates of an individual campaign) with the associated full covariance matrix. Then, normal equations of individual sets are added together and, simultaneously, constraints on the reference frame definition are applied to obtain the final solution. The main advantages of this two-step combination are that (1) the reference frame definition is applied simultaneously and homogeneously to all individual solutions, (2) redundancy of independent observations provides a better estimation of parameters and minimizes possible affects of individual strategies (particularly, it is a powerful tool for detecting outliers), (3) the combination provides a way of comparing and reassessing uncertainties associated with individual solutions, (4) all solutions are expressed in a single consistent velocity frame, and (5) it allows a significant saving in computation time and data storage with respect to a simultaneous analysis of all data.

3.1. Combination of Survey and Continuous GPS Data

[11] We used the CatRef software used for the ITRF calculation to derive a single consistent velocity field using both survey and CGPS solutions. The general combination model is [*Altamimi et al.*, 2002]:

$$\mathbf{x}_s^i = \mathbf{x}_{comb}^i + (t_s - t_0)\mathbf{v}_{comb}^i + \mathbf{T}_s + \lambda_s \mathbf{x}_{comb}^i + \mathbf{R}_s \mathbf{x}_{comb}^i + (t_s - t_0)\left[\dot{\mathbf{T}}_s + \dot{\lambda}_s \mathbf{x}_{comb}^i + \dot{\mathbf{R}}_s \mathbf{x}_{comb}^i\right] \quad (1)$$

$$\mathbf{v}_s^i = \mathbf{v}_{comb}^i + \dot{\mathbf{T}}_s + \dot{\lambda}_s \mathbf{x}_{comb}^i + \dot{\mathbf{R}}_s \mathbf{x}_{comb}^i \quad (2)$$

where $\mathbf{x}_s^i$ is the position vector of point at epoch t_s for survey s, $\mathbf{x}_{comb}^i$ is the final estimated position vector of point i at epoch t_0, $\mathbf{v}_{comb}^i$ is the final estimated velocity vector, $\mathbf{T}_s$, λ_s, $\mathbf{R}_s$ are the transformation parameters between any individual solution s and the combined solution at epoch t_0 for translation, scale, and rotation, respectively, and $\dot{\mathbf{T}}_s$, $\dot{\lambda}_s$, and $\dot{\mathbf{R}}_s$ are their time derivatives. Normalized residuals in the combination solution are used to detect outliers.

[12] Input data for the combination solution are the individual position solutions for each campaign and the CGPS combined position-velocity solution. We also added the full IGS solution for GPS week 1408 in order to strengthen our solution and obtain a better coverage of the Eurasian plate. Minimal constraints were applied homogeneously to all individual loosely constrained solutions. The combination consists in simultaneously estimating the velocity of each site, a seven-parameter transformation between each individual SGPS solution and the combined solution, and a 14-parameter transformation between the CGPS and IGS position-velocity solution and the combined solution.

[13] The quality of a combination relies on the level of redundancy (sites common to several solutions) required to tie the networks together. Only two campaigns (2003 and 2005) were carried out after the CGPS sites had been installed. In order to improve the consistency of our combination, we also constrained the velocities to be equal, within a given uncertainty, for CGPS and campaign sites within 10 km of one another. We did this step in an iterative way, starting with tight constraints (0.01 mm/yr) and carefully checking whether new residuals were in agreement with the imposed velocity constraints. A key aspect of the combination is to give realistic weight to individual solutions. In a preliminary combination step, an a posteriori variance factor $\hat{\sigma}_s^2$ is estimated for each individual solution s following *Altamimi et al.* [2002]:

$$\hat{\sigma}_s^2 = \frac{\mathbf{r}_s^T \mathbf{S}_s^{-1} \mathbf{r}_s}{f_s} \quad (3)$$

where $\mathbf{r}_s$ is the vector of residuals, $\mathbf{\Sigma}_s^{-1}$ the inverse of the variance-covariance matrix for the solution s, and f_s is the redundancy factor given by

$$f_s = 6n_s - tr\left(\mathbf{A}_s \sum\nolimits_{comb}^{-1} \mathbf{A}_s^T \sum\nolimits_s^{-1}\right) \quad (4)$$

where n_s is the number of sites present in solution s, $\sum_{comb}^{-1}$ is the inverse of the variance-covariance of the combined solution, $\mathbf{A}_s$ is the design matrix for solution s contribution to the combination. These $\hat{\sigma}_s^2$ are then applied to each variance-covariance matrix of the individual solutions in an iterative way until both individual $\hat{\sigma}_s^2$ and the global a posteriori variance factor are equal to 1. This procedure therefore enables us to rescale the variance-covariance matrix of each individual solution depending on the average residuals on position and velocities obtained during the combination. We illustrate the effect of the combination on a pair of SGPS and CGPS near Cine (longitude ~28.1°N, latitude ~37.6°N) separated by 10 km. The SGPS site (CINE) benefits from three surveys carried out in 1997.8, 2002.8, and 2005.3 (7.6 years) while the CGPS sites includes 1.7 years of data. The CATS analysis of the CGPS time series provides uncertainties of 1.3, 1.0 and 3.6 mm/yr on the east, north and up components of velocity. The velocity uncertainty derived for the SGPS solutions only is 0.4, 0.5, 5.24 mm/yr on the east, north and up components for the SGPS solutions. The velocity difference between the SGPS and CGPS is 0.2 mm/yr, 1.2 mm/yr and 1.9 mm/yr on the east, north and up components, therefore consistent with the uncertainties. During the combination, both velocities are constrained to be equal at the 0.1 mm/yr level and the weighting algorithm is applied. While the variance-covariance is found to be correct for the CGPS solution, the variance-covariance needs to be rescaled by a factor of about 2 for the individual campaigns included in the determination of CINE. With this rescaling, the SGPS measurements still dominates the final estimated velocity for horizontal velocity, but the final combined estimated velocity has an uncertainty of 0.5 mm/yr for horizontal components and 3.5 mm/yr for the vertical component.

Table 2. Earthquakes With $M_w > 5.5$ That Occurred During the Measurement Period 1997.7–2006.8[a]

	Epicenter				
Earthquake	λ	φ	Date	M_w	Radius (km)
Izmit	29.97	41.01	17.08.1999	7.5	250
Düzce	31.25	40.93	12.11.1999	7.2	200
Cerkes	32.70	40.75	06.06.2000	6.1	40
Sultandagi	31.35	38.40	15.12.2000	5.9	40
Cay	31.21	38.62	03.02.2002	6.1	90
Izmir	26.66	38.15	17–21.10.2005	5.6	40

[a]An offset was estimated simultaneously to the velocity for sites located closer to the epicenter than the distance indicated in radius values.

[14] Finally, we took into account the coseismic displacement caused by six earthquakes with magnitude $M_w > 5.5$ that occurred in the time span (1997–2005) of our data set (Table 2). The October 2005 seismic sequence in Izmir (near the town of Seferhisar) included 4 events with magnitude 5.5–5.9 between the 17th and the 31st of October. The CGPS station located at Mentes (MNTS, 26.72°E, 38.43°N) about 25 km north of the epicenter recorded a 10 mm north displacement over the earthquake sequence. This offset was estimated when calculating the velocity for MNTS. For the other earthquakes, we used a simple approach to correct automatically for any coseismic jump; for sites within a given distance of the epicenter of each earthquake (see Table 2), we added an offset as an additional parameter to be estimated simultaneously with the velocity.

3.2. Combination at Velocity Level

[15] In order to complete our velocity field for western Turkey, we combined our solution with the velocity field from *Reilinger et al.* [2006]. Because we do not have access to the full variance-covariance matrix of positions and velocities of *Reilinger et al.* [2006], we performed a simple combination at the velocity-only level. Covariances between north and east components within each site are taken into account but intersite covariances are neglected. We first expressed our velocity field in a Eurasia fixed reference frame and note that these velocities and those of *Reilinger et al.* [2006] agree to a few tenths of a millimeter per year (RMS difference of 0.4 mm/yr). The two velocity fields were combined using

$$\mathbf{v}_s^i = \mathbf{v}_{comb}^i + \mathbf{R}^i \boldsymbol{\Omega}^i \boldsymbol{\omega}_s \tag{5}$$

where $\mathbf{v}_s^i$ is the horizontal velocity vector expressed in local coordinates of site i in solution s, $\mathbf{v}_{comb}^i$ is the estimated

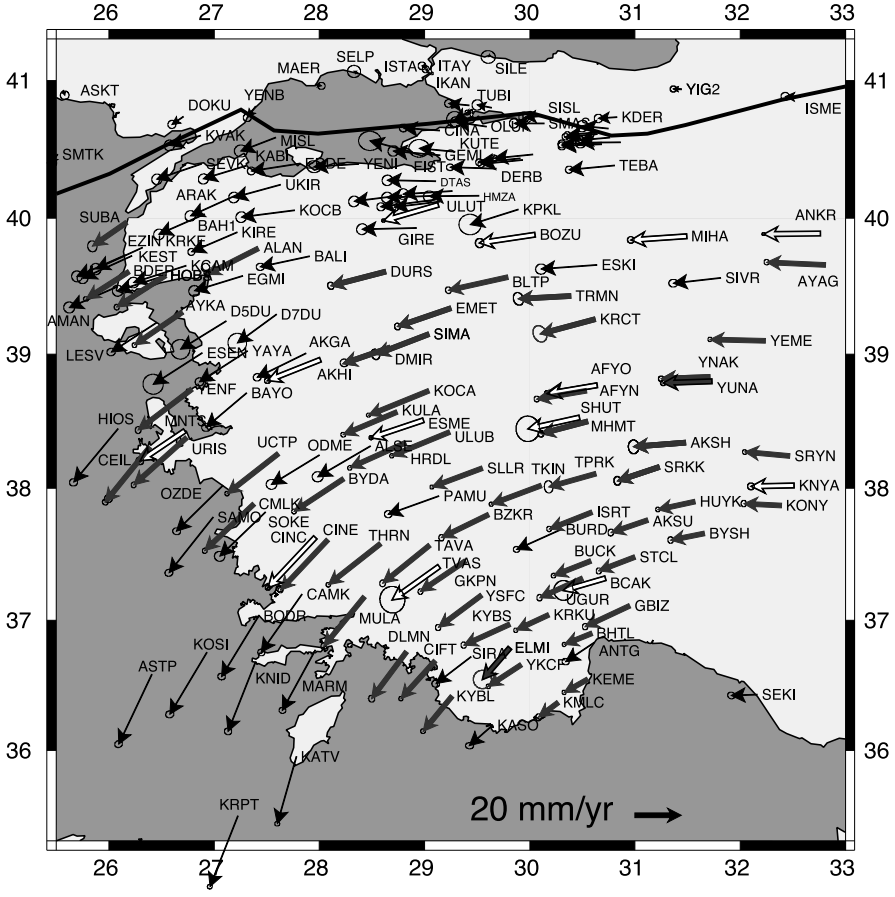

Figure 3. Combined velocity field of western Anatolia with respect to stable Eurasia. Thick grey arrows represent the velocities of survey mode sites determined in the present study. Thick white arrows are velocities at CGPS stations determined in the present study. Thin black arrows represent velocities taken from *Reilinger et al.* [2006] and combined with our velocity field. Error ellipses are at 95% confidence level.

Table 3. Velocity Field Derived in This Study in a Eurasia Fixed Reference Frame

λ[a]	φ[a]	V_e[b]	V_n[b]	σ_{Ve}[b]	σ_{Vn}[b]	σ_{Ven}[b]	site
30.540	38.730	−21.56	−3.58	0.70	0.78	−0.02	afyn
30.644	38.769	−21.42	−2.98	0.51	0.51	0.00	afyo
30.761	40.589	−13.06	−1.14	0.70	0.71	0.00	agok
30.680	40.538	−17.01	−0.63	0.60	0.63	0.01	aguz
27.873	39.006	−21.02	−10.31	0.61	0.59	0.01	akga
28.010	38.960	−22.89	−8.96	0.77	0.74	0.00	akhi
31.480	38.340	−22.44	−1.70	1.40	1.82	−0.05	aksh
31.121	37.762	−16.19	−5.10	0.56	0.54	−0.02	aksu
27.420	39.780	−22.31	−11.17	0.55	0.58	0.00	alan
29.910	31.200	3.74	5.61	1.08	0.85	0.00	alex
28.483	38.315	−22.61	−13.18	0.86	0.80	0.00	alse
26.082	39.501	−20.82	−9.08	0.86	0.87	−0.01	aman
32.760	39.890	−25.66	1.19	0.39	0.33	0.01	ankr
30.609	36.829	−12.19	−8.16	0.57	0.52	−0.01	antg
27.214	40.171	−19.97	−9.04	0.83	0.84	0.03	arak
26.406	36.586	−14.23	−30.03	0.61	0.54	0.03	astp
32.810	39.660	−25.42	1.16	0.68	0.72	−0.01	ayag
26.700	39.311	−19.93	−12.87	0.45	0.45	−0.01	ayka
26.707	39.326	−21.06	−9.80	0.66	0.64	0.00	ayva
26.910	40.029	−19.70	−8.64	0.84	0.84	0.03	bah1
27.906	39.722	−21.20	−4.53	0.64	0.57	0.00	bali
27.308	38.711	−17.44	−14.74	0.69	0.65	0.00	bayo
30.720	37.320	−18.24	−5.23	2.55	2.61	0.00	bcak
26.189	39.614	−19.04	−11.04	0.52	0.49	−0.01	bder
30.590	36.900	−12.01	−4.73	0.53	0.55	0.00	bhtl
29.790	39.570	−25.62	−5.60	0.76	0.89	−0.07	bltp
27.423	37.032	−15.96	−26.08	0.60	0.52	−0.02	bodr
21.040	52.480	0.41	0.33	0.70	0.87	0.00	bogo
17.073	52.277	0.23	0.43	0.36	0.34	0.00	bor1
30.679	40.552	−17.01	−0.63	0.60	0.63	0.01	bozs
30.050	39.880	−23.90	−3.49	1.13	1.22	−0.03	bozu
4.359	50.798	−0.45	−0.31	0.36	0.35	0.00	brus
30.580	37.450	−16.17	−6.24	0.59	0.64	0.01	buck
26.126	44.464	0.27	−0.89	0.42	0.39	0.00	bucu
30.297	37.689	−19.20	−8.63	0.50	0.46	−0.01	burd
28.230	38.070	−21.41	−13.97	0.62	0.66	0.00	byda
31.660	37.660	−14.69	−2.88	0.73	0.87	−0.01	bysh
29.610	37.800	−20.46	−9.84	0.70	0.83	−0.01	bzkr
8.970	39.140	0.74	0.40	0.48	0.43	−0.01	cagl
27.836	37.196	−17.58	−24.98	0.57	0.52	−0.02	camk
29.261	40.200	−21.11	−1.34	0.84	0.84	0.04	cata
26.385	38.311	−18.32	−22.88	0.48	0.48	−0.01	ceil
29.100	36.690	−14.83	−16.22	0.56	0.58	0.00	cift
29.143	40.639	−15.62	1.09	0.64	0.62	0.00	cina
27.960	37.630	−20.45	−21.60	0.67	0.69	0.00	cinc
28.081	37.609	−20.64	−21.16	0.43	0.40	−0.01	cine
27.380	37.880	−21.32	−20.00	0.67	0.69	0.01	cmlk
33.991	44.413	−0.19	0.36	0.57	0.54	0.00	crao
27.112	39.244	−19.64	−12.11	1.50	1.55	−0.01	d5du
27.590	39.295	−16.75	−12.25	1.48	1.49	−0.02	d7du
28.826	36.762	−15.44	−20.07	0.60	0.56	−0.02	dlmn
28.671	39.046	−20.96	−6.51	0.57	0.54	0.02	dmir
23.933	38.079	−15.87	−25.48	0.42	0.40	0.00	dion
26.706	40.739	−4.84	−3.34	0.64	0.64	0.01	doku
35.392	31.593	−2.48	8.90	0.44	0.39	0.01	drag
29.106	40.270	−20.83	0.44	0.83	0.83	0.03	dtas
28.630	39.610	−23.66	−6.02	0.84	0.95	−0.11	durs
27.269	39.577	−20.77	−6.40	0.86	0.85	0.03	egmi
0.490	40.820	0.14	−0.03	0.56	0.57	−0.01	ebre
34.921	29.509	−0.27	9.11	0.42	0.36	0.01	elat
29.810	36.790	−11.94	−13.60	2.37	2.42	−0.06	elmi
35.771	33.182	−2.39	11.05	0.72	0.69	0.00	elro
29.250	39.340	−23.06	−7.82	0.77	0.89	−0.07	emet
27.816	40.400	−20.96	−3.23	0.62	0.61	0.01	erde
26.885	39.010	−21.06	−13.52	1.60	1.58	−0.05	esen
30.637	39.658	−24.01	−1.74	0.87	0.81	0.01	eski
28.990	38.510	−22.64	−7.49	0.55	0.55	0.00	esme
26.317	39.785	−20.05	−9.19	0.86	0.89	0.00	ezin
28.882	40.481	−18.20	4.92	1.79	1.51	−0.04	fist
29.423	40.821	−8.85	0.83	0.61	0.61	0.01	gate
30.950	37.110	−19.34	−8.96	0.71	0.84	0.01	gbiz
29.146	40.460	−20.09	1.83	0.83	0.83	0.03	geml
8.920	44.420	0.64	0.23	0.54	0.55	0.00	geno

Table 3. (continued)

λ[a]	φ[a]	V_e[b]	V_n[b]	σ_{Ve}[b]	σ_{Vn}[b]	σ_{Ven}[b]	site
28.923	39.930	−23.43	−0.54	0.86	0.86	0.04	gire
29.392	37.448	−20.03	−12.24	0.53	0.55	−0.01	gkpn
30.497	50.364	−0.39	0.36	0.38	0.35	0.00	glsv
14.786	49.914	0.70	0.05	0.35	0.34	0.00	gope
6.921	43.755	0.57	0.53	0.37	0.35	−0.01	gras
15.493	47.067	0.77	0.72	0.35	0.32	0.00	graz
28.779	40.167	−20.40	−2.55	0.84	0.84	0.04	haga
0.336	50.867	−0.27	0.77	0.34	0.33	0.00	hers
26.085	38.443	−19.07	−22.96	0.65	0.59	0.03	hios
29.514	40.164	−21.41	−0.19	0.87	0.86	0.04	hmza
26.540	39.580	−21.13	−13.45	0.68	0.75	−0.02	hoba
28.820	38.340	−24.12	−10.71	0.58	0.62	0.00	hrdl
31.570	37.900	−16.14	−3.44	0.58	0.62	0.00	huyk
29.908	40.438	−17.69	−1.75	0.53	0.53	0.00	igaz
104.316	52.219	−0.43	−1.07	0.40	0.41	0.03	irkj
32.570	40.881	−6.47	0.27	0.68	0.62	0.00	isme
30.590	37.820	−18.52	−7.23	0.64	0.72	0.00	isrt
29.929	40.425	−17.69	−1.74	0.53	0.53	0.00	iuck
21.032	52.097	0.15	0.19	0.41	0.43	0.00	joz2
27.301	40.381	−18.24	−5.55	0.80	0.80	0.03	kabi
29.648	36.194	−10.02	−8.76	0.64	0.49	−0.02	kaso
27.781	35.952	−8.21	−28.82	0.40	0.38	0.01	katv
26.732	39.653	−22.65	−7.26	0.85	0.84	0.02	kcam
30.827	40.735	−7.95	−0.52	0.66	0.67	0.01	kder
30.550	36.550	−10.26	−5.66	0.56	0.58	−0.01	keme
26.157	39.731	−20.86	−9.16	0.84	0.86	−0.01	kest
27.217	39.897	−19.62	−8.40	0.55	0.54	0.01	kire
66.885	39.135	0.47	1.42	0.36	0.32	0.03	kit3
30.655	40.628	−13.53	−1.27	0.51	0.52	0.00	kkap
30.745	40.652	−11.17	1.11	0.89	0.91	0.06	kmal
30.270	36.370	−8.60	−6.30	0.79	0.93	0.02	kmlc
27.394	36.681	−11.85	−29.90	0.58	0.54	−0.01	knid
32.510	38.020	−18.60	−0.35	0.90	0.90	−0.01	knya
29.040	38.730	−26.05	−10.49	0.53	0.55	0.00	koca
27.763	40.059	−22.89	−2.94	0.85	0.85	0.03	kocb
32.390	37.870	−16.29	0.82	0.70	0.86	0.01	kony
5.810	52.178	−0.19	0.18	0.35	0.35	0.00	kosg
26.929	36.752	−15.88	−26.53	0.65	0.56	0.03	kosi
29.889	40.066	−20.72	−6.54	1.76	1.62	−0.05	kpkl
30.620	39.260	−23.79	−6.30	1.83	2.16	−0.91	krct
26.216	39.726	−21.11	−9.61	0.86	0.86	0.00	krke
30.180	37.040	−14.30	−6.53	0.56	0.59	0.01	krku
27.224	35.493	−12.00	−30.43	0.39	0.37	0.00	krpt
30.638	40.614	−13.58	−1.21	0.51	0.52	0.00	ktop
28.740	38.570	−23.31	−9.68	0.64	0.64	−0.01	kula
29.288	40.485	−15.40	1.47	1.63	1.40	0.01	kute
26.871	40.601	−13.42	−4.14	0.82	0.85	0.04	kvak
29.260	36.420	−12.55	−15.06	0.62	0.62	0.00	kybl
29.810	36.971	−20.07	−8.73	0.52	0.55	−0.02	kybs
20.670	53.892	−0.95	0.32	0.35	0.33	0.00	lama
26.451	39.234	−19.47	−12.68	0.67	0.59	0.02	lesv
−1.220	46.160	0.09	0.00	0.53	0.53	−0.01	lroc
27.960	40.971	2.72	−0.59	0.59	0.56	0.00	maer
27.963	36.772	−14.23	−25.98	0.53	0.48	−0.01	marm
16.704	40.649	1.17	4.16	0.38	0.37	0.00	mat1
11.647	44.520	2.10	2.04	0.38	0.36	0.00	medi
30.026	40.465	−16.76	−1.68	0.59	0.55	0.00	meke
30.550	38.500	−20.20	−5.23	0.79	0.89	−0.03	mhmt
31.490	39.870	−24.06	−1.59	0.89	0.87	−0.02	miha
27.586	40.588	−15.04	−5.80	1.03	0.95	0.01	misl
26.720	38.430	−19.35	−12.86	1.01	1.01	−0.02	mnts
28.427	37.175	−17.91	−20.94	0.51	0.51	−0.01	mula
−1.690	55.210	0.32	−0.62	0.53	0.60	0.00	morp
33.396	35.141	−6.12	3.37	0.40	0.35	0.00	nico
14.990	36.876	−1.55	4.64	0.42	0.38	−0.01	not1
103.680	1.350	−11.99	2.92	0.76	0.62	0.07	ntus
11.280	48.086	0.35	0.97	0.44	0.43	0.00	obe2
28.000	38.248	−20.62	−12.62	0.84	0.78	−0.01	odme
29.585	40.667	−13.09	1.95	0.85	0.84	0.03	oluk
11.926	57.395	−1.02	0.05	0.34	0.33	0.00	onsa
20.794	41.127	0.85	−2.32	0.63	0.61	0.00	orid
27.085	38.019	−20.01	−19.68	0.62	0.55	−0.02	ozde
11.911	45.385	0.36	1.18	0.46	0.46	0.00	pado

Table 3. (continued)

λ[a]	φ[a]	V_e[b]	V_n[b]	σ_{Ve}[b]	σ_{Vn}[b]	σ_{Ven}[b]	site
29.136	37.941	−21.80	−7.82	0.60	0.57	0.00	pamu
−25.660	37.750	−3.70	−0.64	0.53	0.50	−0.05	pdel
19.282	47.790	1.47	0.38	0.41	0.38	0.00	penc
30.862	40.555	−17.20	−0.15	0.86	0.87	0.03	pina
13.066	52.379	−0.14	0.28	0.36	0.34	0.00	pots
34.763	30.598	−0.86	7.65	0.44	0.42	0.00	ramo
26.989	37.780	−18.97	−23.89	0.63	0.55	0.03	samo
32.160	36.431	−11.13	−0.38	0.57	0.53	−0.02	seki
26.880	40.396	−19.20	−6.57	0.81	0.83	0.02	sevk
−6.206	36.464	−5.04	0.67	0.38	0.36	−0.02	sfer
30.470	38.530	−22.25	−4.86	3.11	3.36	−0.10	shut
29.040	39.150	−23.01	−8.72	1.11	1.37	−0.27	sima
29.439	36.720	−15.12	−11.57	0.61	0.56	−0.02	sira
30.130	40.745	−8.47	−0.65	0.80	0.83	0.00	sisl
31.814	39.564	−20.43	−2.31	0.71	0.61	0.01	sivr
4.680	45.880	0.23	0.34	0.53	0.55	0.00	sjdv
29.550	38.150	−21.86	−8.06	0.53	0.56	0.00	sllr
30.134	40.690	−12.94	0.02	0.71	0.73	0.01	smas
23.395	42.556	0.94	−1.87	0.41	0.37	0.00	sofi
27.486	37.818	−19.66	−18.98	0.82	0.78	−0.01	soke
31.230	38.160	−18.13	−5.98	0.90	1.14	−0.06	srkk
32.470	38.240	−19.47	1.80	0.59	0.62	−0.02	sryn
31.000	37.480	−15.71	−5.93	0.70	0.81	0.02	stcl
26.174	39.973	−16.09	−9.66	0.54	0.51	−0.02	suba
29.048	37.566	−20.76	−15.86	0.59	0.63	0.00	tava
30.804	40.386	−19.55	−1.84	0.57	0.57	0.01	teba
28.580	37.580	−22.53	−17.56	0.59	0.62	0.00	thrn
30.110	38.020	−21.70	−8.00	0.55	0.56	0.00	tkin
1.481	43.561	0.18	−0.05	0.43	0.41	−0.01	tlse
30.630	38.110	−20.52	−5.69	1.16	1.62	−0.15	tprk
30.390	39.430	−22.64	−1.16	1.35	1.67	−0.40	trmn
29.450	40.790	−1.97	−1.18	0.64	0.65	0.00	tubi
24.070	35.530	−16.81	−24.04	1.27	1.23	0.00	tuc2
29.140	37.410	−20.31	−14.33	3.29	3.51	−0.35	tvas
27.610	38.260	−22.15	−17.16	0.59	0.62	0.00	uctp
30.500	37.320	−18.56	−8.36	0.73	0.86	0.02	ugur
27.629	40.245	−20.01	−5.48	0.83	0.84	0.04	ukir
29.141	40.122	−19.44	−2.33	0.71	0.68	0.00	ulda
29.240	38.420	−25.08	−10.18	0.55	0.59	0.01	ulub
29.102	40.136	−23.43	−3.04	0.64	0.63	0.00	ulud
29.130	40.100	−23.61	−6.76	0.46	0.43	0.01	ulut
26.740	38.380	−22.92	−20.31	0.67	0.75	0.00	uris
−3.952	40.444	0.00	0.40	0.37	0.35	−0.01	vill
12.880	49.140	7.57	25.67	1.86	1.15	0.00	wetz
17.060	51.110	−1.18	0.04	0.63	0.65	0.00	wroc
6.605	52.915	−0.19	0.78	0.37	0.37	0.00	wsrt
27.316	39.024	−20.63	−13.31	0.68	0.64	0.01	yaya
32.240	39.100	−24.00	0.62	0.55	0.58	0.00	yeme
27.393	40.811	−3.53	−4.76	0.64	0.61	0.00	yenb
26.790	38.740	−23.26	−17.48	0.77	0.92	−0.01	yenf
28.373	40.398	−19.18	−1.24	1.11	0.95	−0.01	yeni
31.438	40.937	−3.39	0.13	0.50	0.48	0.00	yig2
29.920	36.660	−14.35	−9.26	0.58	0.61	0.00	ykcf
31.710	38.830	−21.02	−0.69	0.70	0.72	0.00	ynak
29.535	37.185	−18.97	−13.55	0.51	0.54	−0.01	ysfc
29.635	40.803	−6.06	1.23	0.85	0.83	0.03	yuhe
31.730	38.800	−21.02	−0.68	0.70	0.72	0.00	yuna
29.111	40.165	−21.26	−0.75	0.84	0.84	0.04	zeya

[a]Longitude and latitude in decimal degrees.
[b]East and north component of velocity with their associated formal errors σ_{Ve}, σ_{Vn}, σ_{Ven} in mm/yr.

combined horizontal velocity vector of site i expressed in local coordinates, $\mathbf{R}^i$ is the transformation matrix from geocentric cartesian coordinates to local coordinates at site i, $\mathbf{\Omega}^i$ is the matrix relating the surface velocity in geocentric cartesian coordinates for site i to an estimate of a rotation vector $\boldsymbol{\omega}_s$ to be applied to solution s. This equation is clearly non invertible and has a rank deficiency of three corresponding to a datum defect of the three rotation rates. The problem is regularized by imposing the constraint that the rotation rates of *Reilinger et al.*'s [2006] velocity field with respect to the combined solution is null. The resulting velocity field is therefore expressed in the same reference frame as *Reilinger et al.* [2006]. We then rescaled the individual variances by applying a rescaling factor to the two solutions. We found a

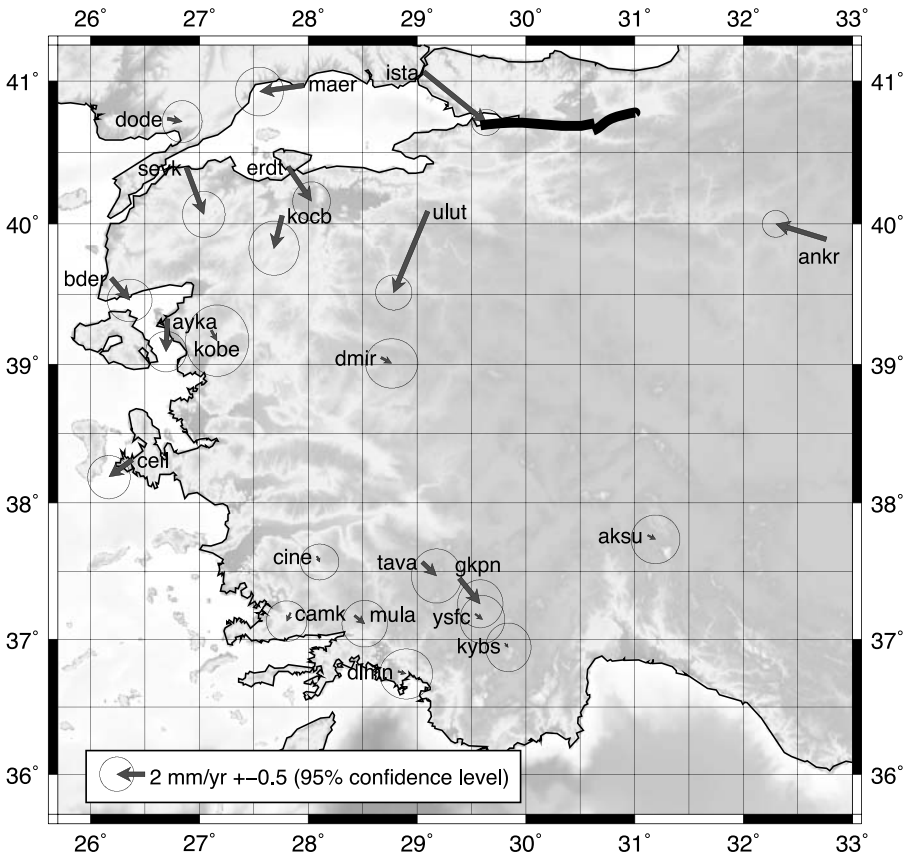

Figure 4. Estimates of the postseismic velocities induced by the Izmit-Düzce earthquakes. Velocities are obtained by subtracting the velocities of *Reilinger et al.* [2006], which are unaffected by the earthquakes, from our velocity field at sites whose velocities are determined including at least three epochs of measurements. The postseismic velocity for the CGPS site ULUT is derived by subtracting the velocity of SGPS site ulda [*Reilinger et al.*, 2006], located 2.6 km from the CGPS site. The velocity at ANKR is the difference between the velocity using 2000–2006 data minus the one derived using 1996–1999 data.

negligible rotation rate between the two velocity fields at the order of 10^{-10} rad/yr, approximately equivalent to 0.3 mm/yr over western Turkey. The values of velocities in the final combined velocity field are listed in Table 3, and the velocity field is illustrated in Figure 3.

4. Analysis of the Velocity Field

4.1. Izmit-Düzce Postseismic Deformation

[16] Most of our velocity field is based on measurements made in the years following the Izmit (17 August 1999 M_w = 7.4) and Düzce (12 November 1999 M_w = 7.2) earthquakes. *Ergintav et al.* [2009] reported postseismic motion as far as ~200 km SE of the Izmit rupture, with highest values within 40 km of the coseismic rupture. We assess the possible impact of the transient deformation following these earthquakes by comparing the velocity derived from our results for the 2000–2005 period with the ones published by *Reilinger et al.* [2006], who, in the Marmara region, used pre-1999 measurements only. Figure 4 shows the differences between the velocities determined by *Reilinger et al.* [2006] and the velocities determined for the SGPS sites during 2000–2005, and for the CGPS sites during 2003–2007. The largest difference (4.4 mm/yr) is found at ULUT, located 65 km from the Izmit rupture. Velocity changes of ~3 mm/yr in a southward direction are found for the sites on the southern coast of the Marmara sea. Farther south, the velocity changes at sites kobe and dmir are found to be below, or close to, 1 mm/yr, roughly the uncertainty of the velocity determination. We also find that immediately after the Düzce earthquake, the westward component of the velocity at ANKR (Ankara), located 180 km from the epicenter became faster by ~3 mm/yr, as found by *Ergintav et al.* [2009]. The distribution of sites common to our solution and that of *Reilinger et al.* [2006] prevents precise delineation of the area undergoing significant postseismic deformation. In the absence of more precise information, we assume that the post-Izmit-Düzce deformation is restricted to a region located north of 39°N. Most of the velocities in this area, however, come from the velocity field of *Reilinger et al.* [2006] and so are not affected by the postseismic deformation. The sites in the affected area whose velocities are determined from our measurements alone are ULUT, BOZU, MIHA, and ANKR (CGPS sites) and suba, alan, durs, and ayag (SGPS sites).

4.2. Methods

4.2.1. Tests of Quasi-Rigid Body Behavior

[17] We use the method described by *Nocquet et al.* [2001] to determine the area of western Turkey that behaves

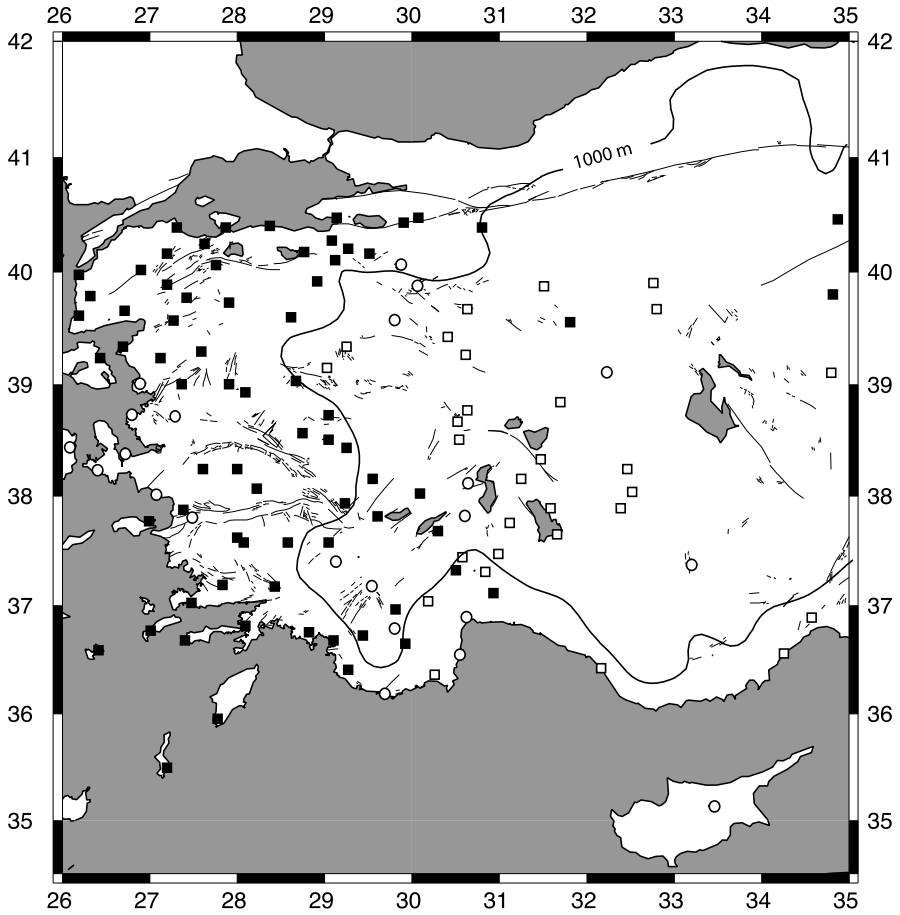

Figure 5. Results of the rigid body analysis of the velocity field. Open squares indicate sites that show no significant deformation with respect to central Anatolia (see text for details). Black squares indicate sites with significant residual velocities with respect to central Anatolia. Open circles indicate sites for which the statistical tests cannot determine whether the motion is consistent with the motion of central Anatolia or not. Thin black line shows the 1000 m height contour, derived from topography smoothed with a Gaussian filter of width 100 km.

quasi-rigidly; this approach does not require any assumption to be made about the location of the boundary of the rigid block. We start by selecting the subset of four sites that provides the minimum variance for the calculated rotation rate vector and the smallest weighted root-mean-square (WRMS) velocity residuals. Once this subset is found, for each remaining site we test, using χ^2, Student and F ratio tests, whether its velocity is consistent with that predicted by the same rigid body rotation rate. If a given site successfully passes the tests, it is added to the core sites used to determine a new rotation rate vector. The test is run iteratively until all remaining sites fail the test. In a second step, all sites are first included in the calculation of a rotation rate vector. We then reject all sites failing the statistical tests described above. The test is run iteratively until all remaining sites pass the test.

[18] As previously found by *McClusky et al.* [2000] and *Reilinger et al.* [2006], this method identifies a region, coinciding with the central Anatolian plateau, in which there is no significant strain (Figure 5). The residual velocities in this region have an RMS of 1.1 mm/yr; this level is consistent with the formal error of our velocity estimates, as indicated by a reduced χ^2 close to 1, and can therefore be considered to be the level of the accuracy of our data set. The region shows a negligible internal strain rate (principal strain rates are 3.5 ± 1.2, 0.9 ± 1.2 nstrain/yr). Sites within 60 km of the North Anatolian fault all show significant residual velocities with respect to central Anatolia. Significant residual velocities are found west of longitude 30.5°E in southern Turkey and west of longitude 29°E for the rest of Anatolia, indicating that the block-like behavior of the Anatolian plateau ends at these longitudes.

4.2.2. Velocity Gradient Analysis

[19] In order to characterize the variations in velocity over western Turkey, we calculate the strain rate and rotation rate fields. We derive strain rates using two different methods. In the first case, we divide the region into small blocks, by subdividing the blocks proposed by *Nyst and Thatcher* [2004] and *Reilinger et al.* [2006] into polygons of area approximately 10^4 km^2. We calculate the velocity gradients assuming constant gradient within each polygon (Figure 6). Velocity uncertainties are propagated in the calculations of strain rate and rotation rate. This simple approach does not require any interpolation of the velocity field and does not smooth the deformation field on the scale greater than the block dimension. If the deformation in western Turkey is

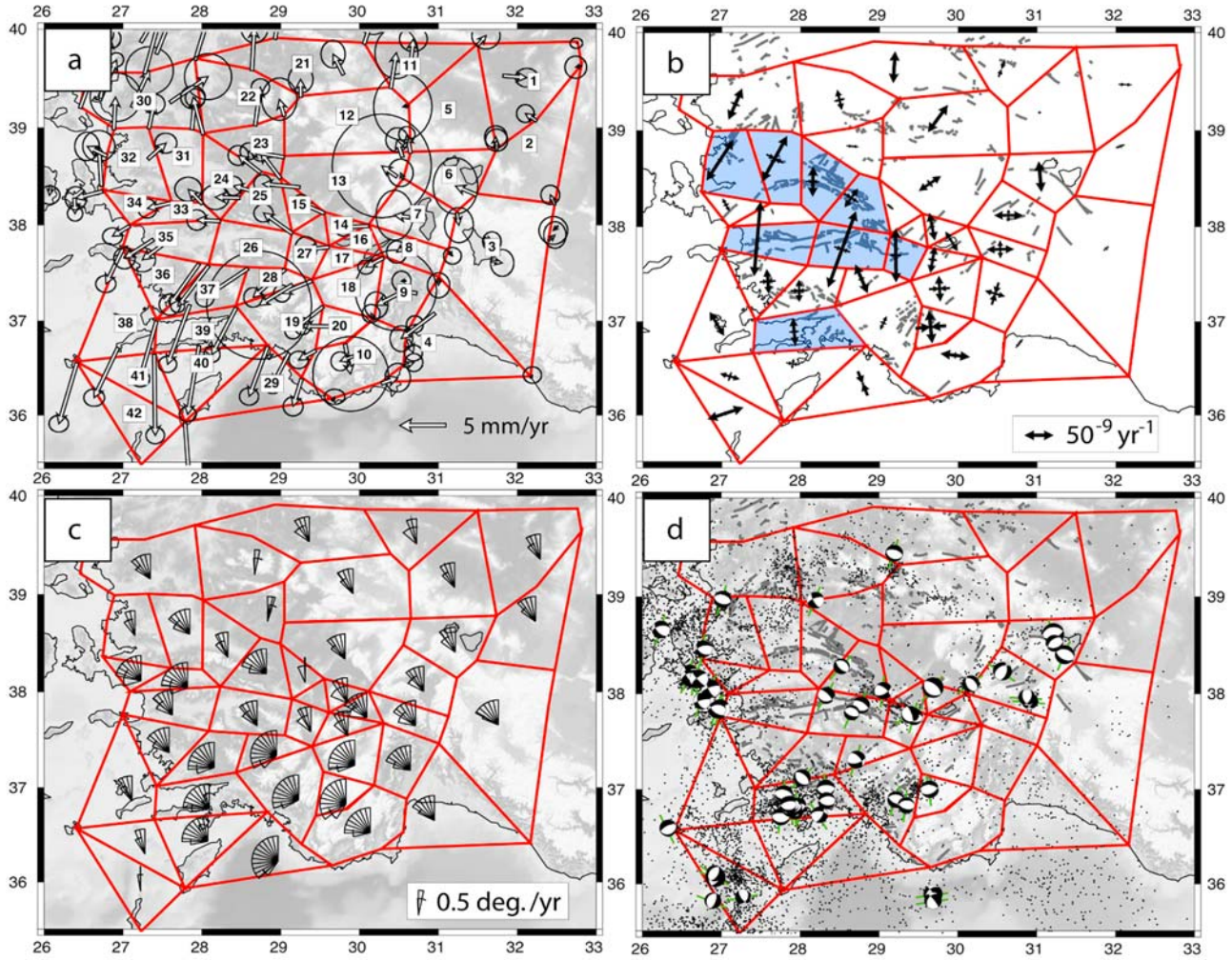

Figure 6. (a) Residual velocities with respect to central Anatolia. Central Anatolia reference frame is defined using the statistical tests described in section 4.1.1. (b) Principal strain rate axes calculated from velocities measured within polygonal regions. All GPS sites within each polygon are used in the calculation. The average misfit for polygons having more than three sites is 1.0 mm/yr (WRMS). Blue background indicates polygons surrounding major active structure chosen by *Nyst and Thatcher* [2004] and *Reilinger et al.* [2006] as major boundaries between rigid blocks. (c) Rotation rates. (d) Distribution of earthquake epicenters from NEIC and Global CMT (http://www.globalcmt.org, $M_w > 4$) for the period 1976–2008.6. Green lines show azimuths of the T axes.

controlled by rigid block rotation, then this method should enable us to detect areas with low strain rates corresponding to block interiors and areas with high strain rates corresponding to the block boundaries.

[20] In an alternative approach, we calculate the strain rate tensor at every node of a regular grid spaced at 17′ in longitude and 13′ in latitude (24 × 24 km). For each node, all sites within 100 km were included in the strain rate estimation, again assuming constant strain rates. We use this method to analyze variations at long wavelength (greater than 100 km) of the strain rate field in western Turkey (Figure 7).

4.3. Characteristics of the Deformation Field

4.3.1. Increase in Extension Rate From East to West

[21] Strain rates of polygons within the central Anatolian plateau (31.5°–33°E) are lower than 5 nstrain/yr, below the uncertainties that follow from the accuracy of the GPS velocity field and confirming the quasi-rigid body test of Figure 5. This observation is further confirmed by the CGPS baseline between Ankara and Konya, which indicates no relative motion at a submillimeter per year level over 3 years of data (0.4 ± 2.3 mm/yr, Figure 2).

[22] Although the test illustrated in Figure 5 shows that the velocities of points in the western Anatolian plateau (29–31.5°E) are consistent, within error, with rigid body rotation of central Anatolia, analysis of the velocity gradients within polygons shows that those velocities are also consistent with a coherent pattern of extension in a N-S to NE-SW direction of the order of 10–20 nstrain/yr (Figure 6). These two statements are not inconsistent. One test (Figure 5) indicates that for the western Anatolian plateau, residual velocities with respect to central Anatolia are individually too small to be statistically distinguished from the rigid body

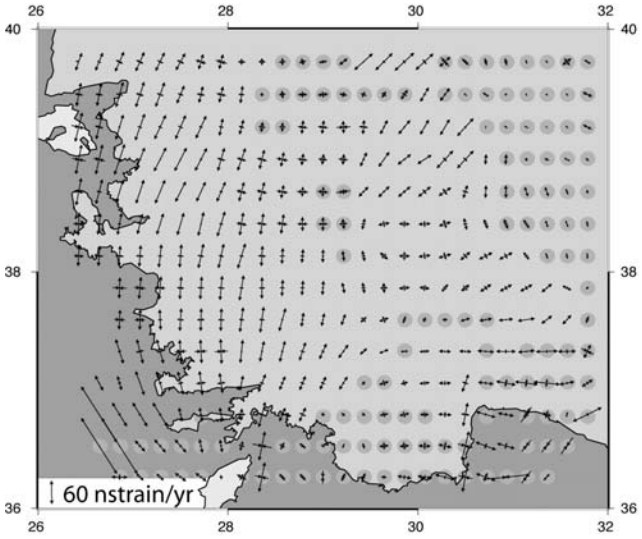

Figure 7. Principal axes of our smoothed strain rate field estimated on a regular 24 × 24 km grid (see text). Grey circles indicate grid points at which the strain rate is not significant according to a χ^2 test. The GPS velocities are fit by this model to a WRMS of 1.3 mm/yr.

motion of central Anatolia. However, the residual velocities are not randomly distributed and the second test (Figure 6) asks whether a group of sites within a polygon exhibits significant velocity gradient.

[23] The rate of extension calculated for the polygons increases from the western Anatolian plateau toward the Aegean coast, with the largest rates being observed across the Gediz graben and Büyük Menderes graben. Extensional rates reach 140 nstrain/yr in the Büyük Menderes graben and 85 nstrain/yr in the Gediz graben at their westernmost extents. If taken up on the grabens alone, these strain rates are equivalent to an opening rate of 6 mm/yr for the Büyük Menderes graben and 4 mm/yr for the Gediz graben. A small component of right lateral motion is also observed for the Büyük Menderes graben. Outside the grabens, we also observe significant extensional strain rates, typically in the range of 40–60 nstrain/yr. This westward increase in the extension rate is clearly seen from the rates of change of baseline length for pairs of CGPS sites (Figure 2). Values of the extension integrated over 400 km from the North Anatolian fault to the Mediterranean coast are -0.5 ± 0.6 mm/yr at longitude 32°E (ANKR-seki), 3.9 ± 1.4 mm/yr at 30°E (BOZU-keme), 14.5 ± 1.2 mm/yr at 28.5°E (durs-dlmn) and 21.8 ± 0.9 mm/yr at 27°E (kire-knid). Note that Figure 4 implies that the influence of the postseismic velocity changes after the Izmit-Düzce earthquakes is to add a component of N-S contraction across this region, so that the conclusion we reach above is not altered by consideration of postseismic deformation.

4.3.2. Long-Wavelength Variations of Strain Rates and Rotation Rates

[24] Figure 7 shows the distribution of the long-wavelength (∼100 km) strain rate field in Turkey. The fit of this smoothed strain rate field provides an WRMS of 1.3 mm/yr. In addition to low strain rates in central Anatolia, as discussed above, strain rates are also low in the area of the Isparta triangle. The rest of the area is dominated by extensional deformation. In the northern half of western Turkey (north of 38°N) the main direction of extension is NE-SW to NNE-SSW. This direction rotates counterclockwise as one moves southward, becoming NNW-SSE in the southeastern Aegean. Rotation rates derived from the GPS velocities are approximately constant and counterclockwise in the central and western part of the Anatolian plateau (Figure 6c). Larger counterclockwise rates are observed in southwestern Turkey. The change in velocity direction in that area results therefore from a combination of extension and increasing rotation rates.

4.3.3. Strain Rates and Earthquakes in Western Turkey

[25] At least six earthquakes with magnitude greater than 6 occurred within this area during the 20th century [*Ambraseys and Jackson*, 1998] and several of them occurred in areas where no block boundary has so far been proposed, such as the 1970 Gediz earthquake (M_w = 7.1), the 1995 Dinar earthquake (M_w = 6.1) and the Sultandagi (M_w = 6.1) earthquake. Figure 6d shows the focal mechanisms from the Global CMT catalog between 1976 and 2008. All focal mechanisms show a very good agreement between the sense of faulting and the principal strain rate axes derived from the GPS velocities. Change of the direction of extension from NNE-SWW in northwestern Turkey to SE-NW in southwestern Turkey is seen in both geodetic data and focal mechanisms. Both the occurrence of these large earthquakes, and the strain rates observed by GPS, indicate that strain is not limited to the block boundaries proposed in previous studies.

4.4. Elastic Block Models

[26] *Nyst and Thatcher* [2004] and *Reilinger et al.* [2006] concluded that the kinematics of the central Anatolian plateau and western Turkey could be simply modeled by the rigid body relative rotation of a small number of blocks. Our denser velocity field enables us to revisit this question and quantitatively assess the conclusions of those studies. We use an approach similar to that of *Meade et al.* [2002], in which we simultaneously estimate the rotation vectors for each block. Interseismic elastic loading along faults defining the blocks boundaries is accounted for during the inversion by correcting the velocities within each block by an amount of "back slip" [*Savage*, 1983]. Our inversion scheme uses the simplex algorithm to minimize a cost function defined as the sum of the absolute value of the residuals (L1 norm), weighted by the formal errors in the velocities. Using the L1 norm rather than a classical least squares method (L2 norm) reduces the impact of potential outliers on the estimated parameters. All faults are assumed to be vertical, and extensional boundaries are modeled by a tensile source [*Okada*, 1985]; while this model is only an approximation to the deformation associated with normal faults, comparison with the interseismic deformation generated by a normal fault dipping at 45° shows difference less than 20% at a distance twice the locking depth from the fault in the hanging wall and less than 5% in the footwall.

[27] A block description of the kinematics explicitly assumes that the strain rate occurring within the interiors of blocks is significantly smaller than the strain rate within a distance from the block boundaries that is a few ($\sim\pi$) times the thickness of the elastic upper crust. To assess the

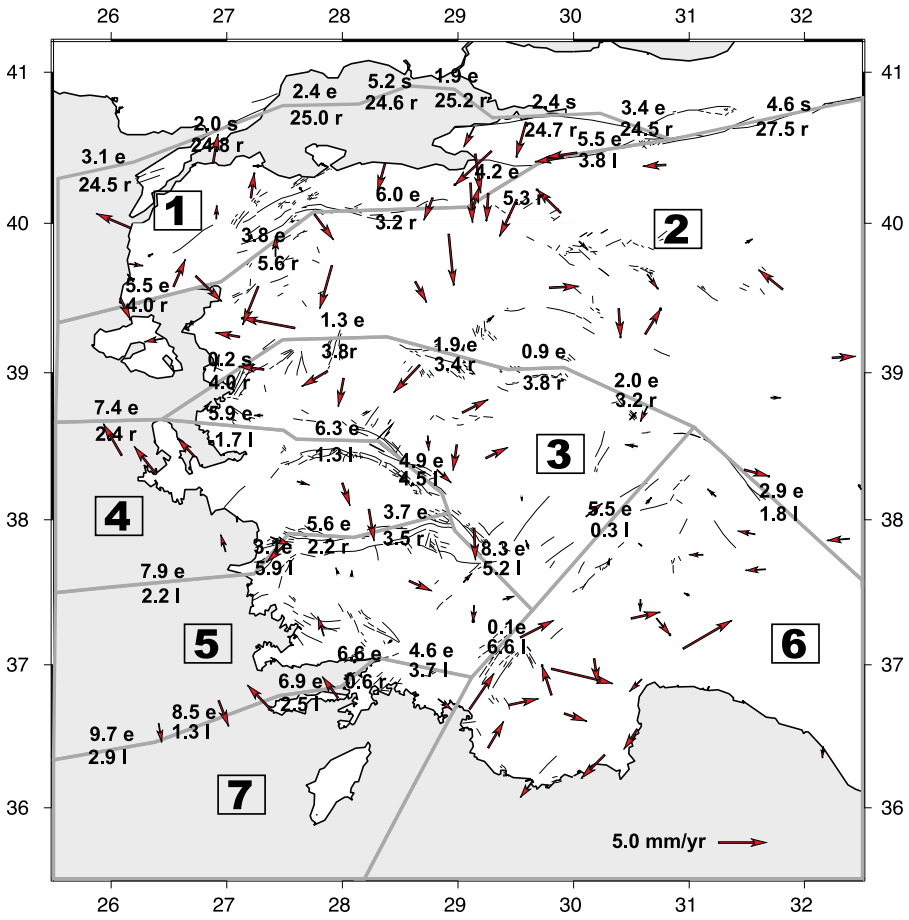

Figure 8. Kinematic elastic block model of western Turkey. Block boundaries are shown in grey lines. Slip rates predicted along boundary segments are indicated in mm/yr; e, extension; s, shortening, l, left-lateral strike slip; r, right-lateral strike slip. Arrows show residual velocities (observed-modeled).

performance of each block model, we therefore provide both the weighted root-mean-square (WRMS) residual velocity, and the average residual strain rate within each block. We estimate the residual strain rate from the difference between observed and modeled velocities for each block; that is, the residual strain rate for each block interior has been corrected for the strain rate along block boundaries that arises from the assumed interseismic elastic loading.

[28] *Nyst and Thatcher* [2004] proposed a model involving three blocks (Marmara, Anatolia and South Aegean). Using their geometry, we find an overall misfit of 2.6 mm/yr, with a maximum WRMS residual velocity of 3.4 mm/yr for the South Aegean block. *Reilinger et al.* [2006] used a similar geometry, except that (1) their boundary between Anatolia and the Aegean follows the Gediz graben while *Nyst and Thatcher* [2004] chose instead the Büyük Menderes graben as the main boundary and (2) an additional block was introduced in southwestern Turkey (South Aegean block). *Reilinger et al.*'s [2006] model provides a better fit to the observed GPS data, with an overall WRMS residual velocity of 1.9 mm/yr. However, residual velocities reach 7 mm/yr in western Turkey as Reilinger et al. noted. In each model, central Anatolia shows insignificant internal deformation, with WRMS residual velocity of 1.1 mm/yr and strain rate < 5 nstrain/yr. The strain rate field in westernmost Turkey shows extension rates as large as 40 nstrain/yr for the Aegean and Anatolian blocks south and north of the Gediz graben. We therefore conclude that if a block model is to account for the velocity field in western Turkey, more, smaller blocks are required than those used by *Nyst and Thatcher* [2004] and *Reilinger et al.* [2006].

[29] In an attempt to produce such a fit, we define additional blocks by dividing the blocks within which significant strain rates had been found. We use the distribution of seismicity (Figure 1) and active fault maps [*Saroglu et al.*, 1992] as additional guides. In the block models of *Nyst and Thatcher* [2004] and *Reilinger et al.* [2006], significant extension rates were found north of the Gediz graben. We define an additional boundary following the Simav fault zone which caused the 1969 Demirci earthquake [*Eyidogan and Jackson*, 1985], prolonging it east to the epicenter of the M_w = 7.1 Gediz earthquake, and joining the apex of the Isparta block along the Afyon fault. Large extensional rates observed along the southwestern Aegean coast and the islands of Rhodos, Kos, Astipalaia, and Karpathos islands support an additional boundary in southwestern Turkey, and we find that the best fit to the data is achieved using the boundary proposed by *Reilinger et al.* [2006] that follows the southern coast of the Gököva gulf. Marginal improvements are found adding a boundary following the Eskesehir fault and joining

Table 4. Euler Vectors Relative to Eurasia for the Blocks Defined in Figure 8[a]

λ	ϕ	$\dot{\omega}$	σ_1	σ_2	*azim.*	$\sigma_{\dot{\omega}}$	*WRMS*	*N*	Polygon
29.34	33.02	1.584	0.31	0.05	62	0.073	1.40	23	1
31.62	32.07	1.602	0.39	0.06	46	0.041	1.40	31	2
31.83	31.44	1.726	0.61	0.06	78	0.085	1.27	18	3
34.86	30.71	1.512	0.51	0.05	165	0.175	1.52	10	4
33.27	33.29	2.636	0.15	0.03	−172	0.114	0.90	12	5
32.56	34.03	2.406	0.12	0.03	106	0.079	1.56	25	6
32.97	34.69	3.616	0.21	0.03	−103	0.237	1.37	4	7

[a]The λ,ϕ longitude, latitude in decimal degrees. $\dot{\omega}$ is the angular velocity in decimal degree per Ma. σ_1,σ_2 are the one-sigma lengths in degrees of the semimajor and semiminor axes of the Euler vector ellipse; *azim* is the azimuth of the semimajor ellipse axis in degrees clockwise from north. $\sigma_{\dot{\omega}}$ one-sigma error on $\dot{\omega}$. WRMS, weighted root-mean-square of the residual velocities in mm/yr. *N* is the number of sites in each block used for the Euler vector calculation. Polygon is the polygon number shown in Figure 8.

the southern strand of the North Anatolian fault, and splitting the Isparta triangle block in two subblocks, but we do not present this solution.

[30] Our block model (Figure 8 and Table 4), divides western Turkey into six blocks with an approximately equal width of 80 km, the smallest size of blocks we can resolve with a ∼50 km dense velocity field. This increase in the number of blocks results in a reduction of the WRMS residual velocity to 1.7 mm/yr, but highly significant internal strain rates are found for four of the seven blocks. Strain rate close or above 30 nstrain/yr are found for at least three blocks (Table 5).

[31] The residual strain rates of 30 nstrain/yr within our smaller blocks should be compared with the largest modeled strain rates near the block boundaries, which are found in the westernmost Büyük Menderes graben (140 nstrain/yr) and in the Gediz graben (85 nstrain/yr). Farther east, block boundary strain rates are 40–50 nstrain/yr, only slightly larger than average strain rate occurring within blocks. In western Turkey, other than close to the North Anatolian fault, the strain rates calculated as arising at the boundary between blocks are at most 3–5 times larger than the strain rates occurring within blocks. We therefore do not concur with the conclusion of *Nyst and Thatcher* [2004] that strain rates at blocks boundaries are 1 or 2 orders of magnitude larger than strain rates within block interiors.

5. Discussion

[32] One of the objectives of determining detailed continental velocity fields is to find the most economical and physically simple means of describing continental deformation. We have investigated here the description that approximates the velocity field by the relative rotation of rigid blocks and accounting for the interseismic contribution induced by the locking of faults at crustal depths. This kinematic description is physically equivalent to a model where faults slip continuously beneath an elastic lid. It is physically simple, and economical provided that the number of blocks is small. This hypothesis explicitly assumes that the strain rates occurring within block interiors are significantly smaller than those occurring close to the bounding faults. We find that on the contrary, the residual strain rates within blocks in western Turkey are on average above 20 nstrain/yr and sometimes no more than a factor of 2 or 3 smaller than the strain rates near the boundaries. We note that such strain rates, sometimes regarded as negligible in discussions of blocks, are equivalent to a fault slipping at 1–2 mm/yr in each of the ∼30 polygons of Figure 6 where residual strain rates of this magnitude are found. Such faults, capable of yielding a magnitude 6 earthquake every couple of centuries, are responsible for much destruction in this region.

[33] It must always be possible at some scale to find a description of the motion in terms of blocks, if only at the scale of the spacing between individual faults of the region (∼15–40 km). Our results show that within western Turkey, the blocks must be less than 80 km wide. If we were to reduce the linear dimensions of the blocks by a factor of 2 from 80 to 40 km, the number of blocks would increase from 7 to about 30. But the elastic block model predicts strain near the block boundaries, caused by the slipping of dislocations below the seismogenic layer. If that layer is ∼15 km thick, then the block boundary deformation is spread out over about 40 km either side of each boundary, and for 40-km blocks, the surface velocity field would vary smoothly, giving no indication of the existence of the blocks. For interseismic deformation, there would be no effective difference between a description in terms of blocks and one in terms of distributed deformation.

[34] We illustrate this point by focusing on the region of rapid extension in western Turkey, between 26°E and 30°E, which forms approximately half of our study area. Here, while some of the major fault systems are represented by the block boundaries proposed by *Reilinger et al.* [2006], and others by those of *Nyst and Thatcher* [2004], several fault systems, marked by large earthquakes and with clear geomorphic expressions, are a considerable distance from any such boundary (Figure 1).

[35] These fault systems could be incorporated into a block model by introducing more boundaries (see above), but an alternative is suggested by the observation that the azimuths of the T axes of the earthquakes in western Turkey

Table 5. Residual Strain Rate Within Each Block Defined in Figure 8[a]

Eps1	Eps2	Azimuth	χ^2	Polygon
26.9 ± 8.0	−6.9 ± 5.0	68.8 ± 6.9	27.6	1
1.3 ± 1.0	−2.1 ± 2.4	−0.5 ± 21.0	2.9	2
5.7 ± 2.6	−9.9 ± 3.5	37.3 ± 9.9	10.5	3
37.7 ± 7.2	−13.3 ± 8.4	40.1 ± 6.6	40.1	4
8.2 ± 7.1	6.6 ± 8.1	33.9 ± 17.2	6.7	5
11.5 ± 2.9	−19.5 ± 2.7	83.0 ± 3.4	89.2	6
53.4 ± 8.7	2.2 ± 8.7	40.8 ± 6.1	44.0	7

[a]Eps1 and Eps2 are the principal strain rates in nstrain/yr; The azimuth of Eps2 is given in decimal degrees; χ^2 indicates the result of a χ^2 test of significance of the strain rate tensor. The threshold value for at a 99% confidence level is 11.35.

cluster tightly about the N-S direction in western Turkey, whether or not they lie on block boundaries (Figures 1 and 6). This observation, taken with the fact that the principal axes of horizontal extension calculated from the GPS velocities are also aligned with the same direction (Figures 6b and 7), raises the question of whether it may be simpler to explain the combined data set of GPS velocities, earthquakes, faulting, and geomorphology by the distributed strain of the brittle crust rather than by the rotations of a set of blocks.

[36] In a frame of reference that minimizes velocities in the region 26°–30°E, 36°–40°N (Euler pole at longitude 35.25°E, latitude 30.24°N, angular velocity 1.348 deg/Ma), the GPS velocities in western Turkey show clearly the extension in a N-S direction (Figure 9). In that reference frame, the east component of velocities do not show any significant variation others than the shear associated with the North Anatolian Fault system. Along a N-S profile, velocity southward component shows smooth increases (Figure 9a). The key point about this observation is that while variations in the component of velocity perpendicular to the profiles may reflect either rigid body rotation or strain, the gradients of north component of velocity shown in Figure 9b must represent only strain, as proved in Appendix A. We now investigate the degree to which the elastic block model matches this N-S strain.

[37] A purely rigid block model predicts that the N-S profile would consist simply of a number of steps in velocity (Figure 9c). The constant value of the along-profile component of velocity within each block, despite variations in distance from the pole of rotation, is the property of rigid body rotations referred to above (and see Appendix A). Step-like behavior in velocity would occur on intersesimic timescales only if the bounding faults slipped freely at the surface. If the effect of locking of the faults during the interseismic phase is taken into account, the change of velocity from one block to another is smoothed over a distance of approximately twice the locking depth or typically ~30 km in this region (Figure 9d). This elastic block model still predicts large strain rates across the boundaries of blocks, and low strain rates in the middle of blocks.

[38] However, the N-S velocity profiles shown in Figure 9b show no clear evidence either of abrupt changes in velocity or of areas of low strain rate. On the contrary, a smooth velocity gradient is observed, with a constant strain rate of 50 nstrain/yr, decreasing at the northern end of the profile, near the North Anatolian fault. This average extensional rate does not exclude more local variations in strain rate as shown in Figure 6b, but suggests that models with relatively smooth velocity variations are likely to provide fits similar or better to block models. Indeed, a single rotation rate plus a linear velocity gradient, i.e., uniform N-S extensional strain rate (Figure 9e), provides a fit of WRMS = 2.9 mm/yr, versus 3.6 mm/yr for the four block model proposed by *Reilinger et al.* [2006]. A model including four elastic blocks has twelve parameters (three components of a rotation rate for each block and assuming a fixed locking depth for all faults), while our uniaxial extension model only has four parameters (a rotation rate vector and a constant N-S extension rate). The simple uniaxial strain rate model therefore provides a better fit with fewer parameters than others block models. This result, together with the considerations described above, suggests that for western Turkey at least, crustal deformation may be described as that of a continuum, certainly for length scales greater than 1 or 2 times the thickness of the seismogenic layer.

[39] If the lithosphere is treated as quasi-continuous, then it is a simple matter to relate the instantaneous strain rates to the finite strain over geological time spans. We illustrate this point by considering the relationship between extensional strain rate and crustal thickness across western Turkey. In Figure 10a, we plot the N-S rates of extension in western Turkey averaged between 40.5°N and 36°N as a function of longitude. Figure 10b shows estimates of crustal thicknesses from receiver function studies [*Saunders et al.*, 1998; *Sodoudi et al.*, 2006]. We interpolate between the sparsely distributed crustal thickness measurements by assuming that the topography, averaged in a north-south direction, is (Airy) isostatically compensated by crustal thickness variations.

[40] The decrease in crustal thickness westward from the central Anatolian Plateau occurs in the same longitude range as the increases in north-south extensional strain rates (Figure 10). Assuming extension of an incompressible crust, the rate of change of crustal thickness is given by

$$\frac{dC}{dt} = \dot{\varepsilon} C \tag{6}$$

where C is the crustal thickness and $\dot{\varepsilon}$ is the rate of vertical strain, which (neglecting east-west strain) we take to be the negative of the north-south extensional strain rate. Assuming $\dot{\varepsilon}$ constant with time, the solution of this equation is

$$C = C_0 \exp(\dot{\varepsilon} t) \tag{7}$$

where C_0 is the crustal thickness at the onset of extension. *Dewey and Sengör* [1979], *Angelier et al.* [1981], and *Jackson and McKenzie* [1988] indicate that extension in the major grabens may have started in middle or late Miocene, but became widespread and rapid by the Pliocene (circa 5 Ma). Assuming that the extension in Turkey began about 5 Ma, we calculate the present-day crustal thickness as a function of longitude, using an initial crustal thickness C_0 of 37.5 km, the thickness of the crust in the central Anatolian plateau near Ankara [*Saunders et al.*, 1998], and the observed average rates of extension (Figure 10a). The calculated values of crustal thickness track well the observed values (Figure 10b), suggesting that the distribution of crustal thickness in western Turkey reflects the extension of a region of initially constant crustal thickness for several million years, at strain rates which (like today's field) increase from low values in central Anatolia, to ~60 nstrain/yr near the Aegean coast.

[41] The mechanism controlling the observed strain rate field has yet to be clarified. Westward motion of Anatolia is directed from the high topography in eastern Turkey and the Caucasus mountain range toward the low topography along the Hellenic trench. Velocities expressed in the central Anatolia reference frame (Figure 6) show that the magnitude of velocity increases as the distance from the trench decreases. This observation supports a model in which the continental lithosphere of western Turkey responds to a gradient in gravitational potential energy, between the Anatolian plateau and the trench, by flowing southwestward

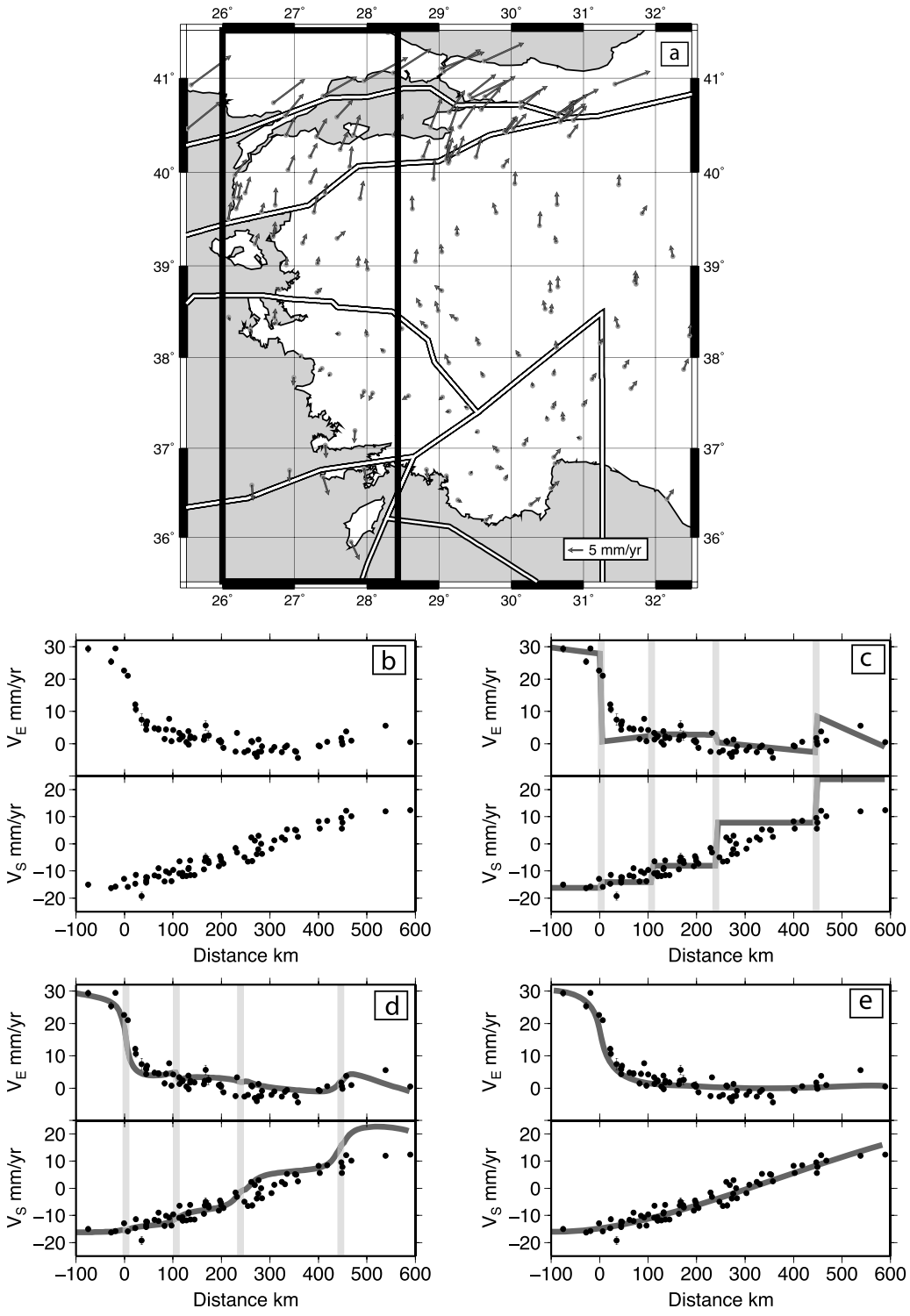

Figure 9. (a) Velocities of the sites in western Turkey, after the removal of an average rigid body rotation (Euler pole at longitude 35.25°E, latitude 30.24°N, angular velocity 1.348 deg/Ma). Double lines show the block boundaries of *Reilinger et al.* [2006]. Sites included in the black rectangle were used to produce the profiles. (b) South and east components of velocity as a function of the distance to the North Anatolian fault. (c) Velocity components predicted by the rigid rotation of blocks proposed by *Reilinger et al.* [2006]. (d) Same as Figure 9c with the interseismic contribution of elastic strain caused by faults locked at 10 km depth. (e) Velocity components predicted by a model including the elastic strain caused by the Anatolian faults locked at 15 km depth and a constant 50 nstrain/yr N-S extensional strain rate. The WRMS are 6.0 mm/yr for the rigid block model (Figure 9c), 3.6 mm/yr for the elastic block model (Figure 9d), and 2.9 mm/yr for the model (Figure 9e). Grey bars indicate the places where the block boundaries of *Reilinger et al.* [2006] intersect the profiles.

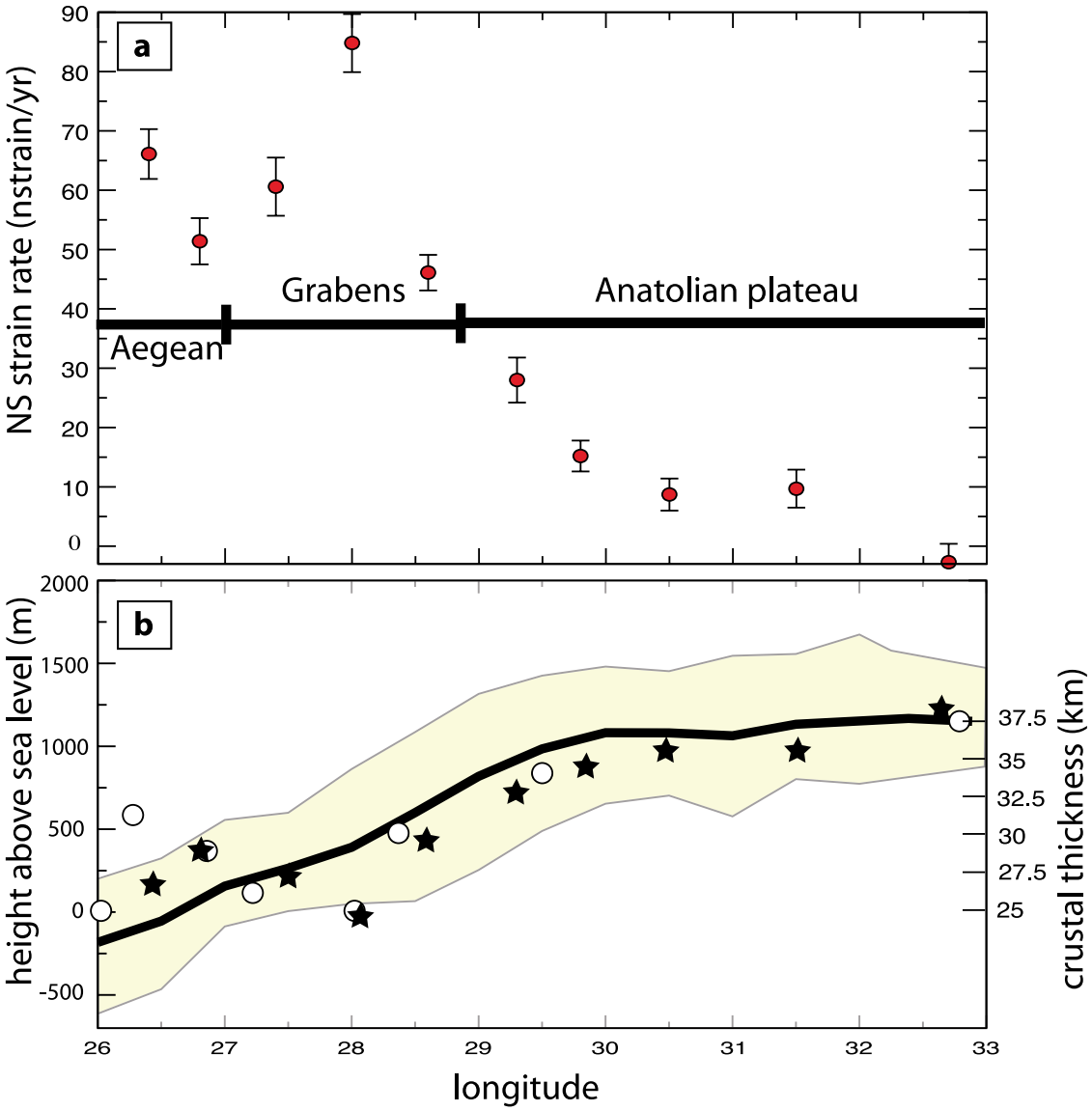

Figure 10. (a) North-south extensional strain rates averaged across N-S swaths of western Turkey, south of the North Anatolian fault, plotted as a function of longitude. (b) Observations of surface height and inferences of crustal thickness across the same region. Black line shows average surface height, with the grey band showing maximum and minimum heights. Open circles show crustal thicknesses from receiver function studies in western Turkey [*Saunders et al.*, 1998; *Sodoudi et al.*, 2006]. Blacks stars show crustal thicknesses calculated (at the longitudes for which extensional strain rates are calculated in Figure 10a) by applying the observed extension rates at these longitudes for 5 Ma, starting with a crustal thickness of 37.5 km, which is the present-day value in central Anatolia.

toward the region of lower potential energy [e.g., *McKenzie*, 1972; *Le Pichon*, 1982]. Detailed consideration of the dynamics of this deformation is beyond the scope of this paper and will be addressed elsewhere.

6. Conclusions

[42] Our study provides an extensive, accurate geodetic velocity field in one of the most rapidly extending regions of the continents, which is derived from a rigorous combination of both continuous and survey-type GPS measurements. With an accuracy around 1 mm/yr and an intersite spacing of ~50 km, it provides a critical data set for discriminating between models of the tectonics of the region.

[43] There is a clear concentration of strain rate in the region a few tens of kilometers either side of the North Anatolian fault, where strain rates reach 400–600 nstrain/yr [*McClusky et al.*, 2000; *Reilinger et al.*, 2006]. While no deformation is resolved at the precision of our data set in the central Anatolian plateau, the western part of the plateau shows extension rates of ~20 nstrain/yr, and rates increase across the grabens of western Turkey to the Aegean coast, where they reach a mean value of about 60 nstrain/yr. As reported by *McClusky et al.* [2000] and *Reilinger et al.* [2006], the integrated N-S extension rate at longitude 27°E

exceeds 20 mm/yr, a rate that is comparable to the 20–25 mm/yr right-lateral shear across the North Anatolian fault. The portion of the extension that is accommodated across the major grabens along the Aegean coast (Gediz, Küçük/Büyük Menderes grabens) is 11.0 mm/yr as shown by the time series between the two CGPS sites AKHI and CINC (Figure 2), and is similar in magnitude to the opening rate of the Gulf of Corinth [*Clarke et al.*, 1998; *Briole et al.*, 2000]. That extension probably also occurs offshore farther south, as is suggested by marine geophysical survey results [*ten Veen et al.*, 2004]. To within the precision of our observations, western Turkey can be considered as an area in which extension increases smoothly from the central Anatolian plateau to the Aegean coast (Figures 9 and 10).

[44] As others have suggested [e.g., *Reilinger et al.*, 2006] the contrast between the rapid strain near the North Anatolian fault and the slow internal deformation (<5 nstrain/yr) of the Anatolian plateau in central Turkey provides strong support for the model of continual slip in a narrow zone beneath a lid of elastic blocks. In western Turkey south of the North Anatolian fault, however, our several attempts to model the velocity field by the rotation of a limited number of elastic blocks with slipping faults around their edges are unsuccessful, contradicting previous conclusions based on sparser velocity fields, that block models can account for the deformation of the region.

[45] Our results show that even if a good fit to the velocity field of western Turkey can be found by introducing more blocks, they would need to be appreciably smaller than ~80 km, and hence would be so numerous that the block description could no longer be regarded as economical. Furthermore, once the blocks become smaller than a few times the thickness of the seismogenic layer (~50 km), there is no effective difference between the interseismic velocity field of the elastic blocks and that of a continuum (section 4.4). Finally, a block model that was tied to faults spaced apart by only a few tens of kilometers would have limited explanatory or predictive power, given the evidence that individual fault systems in the region migrate on the timescale a few hundred thousand years [e.g., *Goldsworthy and Jackson*, 2000].

[46] An alternative explanation for the distributed upper crustal strain in western Turkey is that apart from the neighborhood of the North Anatolian fault, strain beneath the upper crust is not confined in narrow bands beneath a small number of block boundaries, but is distributed more widely throughout the lower lithosphere. In this interpretation, the upper crust would follow the strain of the lower lithosphere, releasing the strain by slip on faults, some, but by no means all, of which are the faults with clear geomorphic expression. This explanation receives support from the observation that the T axes of the $M_w \geq 6$ earthquakes of the region are aligned with the extensional principal axes of the distributed strain field, irrespective of whether they occurred on the boundaries or the interiors of the postulated large blocks (Figure 6). This explanation also allows a calculation of the finite strain of the region; if we assume that the crust of the region had approximately constant thickness at 5 Ma then the strain rates measured by GPS account for the present-day distribution of crustal thickness in western Turkey (Figure 10).

[47] Irrespective of the details of the strain distribution in the lower lithosphere of western Turkey, we favor the dynamical model that explains the region's westward and southward motion, and its distributed extension, as the response of a deformable lithosphere to gradients of gravitational potential energy within it, and to tractions applied at the Hellenic subduction zone [*McKenzie*, 1972, *Le Pichon*, 1982].

Appendix A

[48] We provide a proof of the result seen in Figure 9c and commented on in the discussion that the component of the velocity due to a rigid body rotation pointing along a great circle is invariant along that great circle.

[49] The velocity due to a rigid body rotation is given by

$$\mathbf{v} = \dot{\boldsymbol{\omega}} \times \mathbf{r} \tag{A1}$$

where $\mathbf{v}$ is the velocity, $\dot{\boldsymbol{\omega}}$ the rotation rate vector, and $\mathbf{r}$ the vector position on the Earth's surface, taking the Earth's center as the origin. This expression may also be written

$$\mathbf{v} = R\left(\dot{\boldsymbol{\omega}} \times \hat{\mathbf{r}}\right) \tag{A2}$$

with R the radius of the Earth and $\hat{\mathbf{r}}$ the unit radial vector pointing at the position at which the velocity is being determined.

[50] We restrict attention here to the case of the variation of the northward component of velocity in a north-south direction. The northward component of velocity is

$$v_n = R\left(\dot{\boldsymbol{\omega}} \times \hat{\mathbf{r}}\right) \cdot \hat{\mathbf{n}} \tag{A3}$$

where $\hat{\mathbf{n}}$ is the unit vector tangential to the Earth's surface at $\mathbf{r}$ that points northward.

[51] Consider the derivative of v_n with respect to latitude φ

$$\frac{\partial v_n}{\partial \varphi} = R\left(\dot{\boldsymbol{\omega}} \times \frac{\partial \hat{\mathbf{r}}}{\partial \varphi}\right) \cdot \hat{\mathbf{n}} + R\left(\dot{\boldsymbol{\omega}} \times \hat{\mathbf{r}}\right) \cdot \frac{\partial \hat{\mathbf{n}}}{\partial \varphi} \tag{A4}$$

[52] The unit vectors $\hat{\mathbf{r}}$ and $\hat{\mathbf{n}}$ are given by

$$\hat{\mathbf{r}} = \cos\varphi\, \mathbf{i} + \sin\varphi\, \mathbf{k} \tag{A5}$$

$$\hat{\mathbf{n}} = -\sin\varphi\, \mathbf{i} + \cos\varphi\, \mathbf{k} \tag{A6}$$

where $\mathbf{k}$ is the unit vector along the Earth's rotation axis and $\mathbf{i}$ the unit vector along the intersection of the equatorial plane and the meridian. The derivatives of $\hat{\mathbf{r}}$ and $\hat{\mathbf{n}}$ are therefore given by

$$\frac{\partial \hat{\mathbf{r}}}{\partial \varphi} = -\sin\varphi\, \mathbf{i} + \cos\varphi\, \mathbf{k} = \hat{\mathbf{n}} \tag{A7}$$

$$\frac{\partial \hat{\mathbf{n}}}{\partial \varphi} = -\cos\varphi\, \mathbf{i} - \sin\varphi\, \mathbf{k} = -\hat{\mathbf{r}} \tag{A8}$$

and

$$\frac{\partial u_n}{\partial \varphi} = R\left(\dot{\omega} \times \hat{\mathbf{n}}\right) \cdot \hat{\mathbf{n}} - R\left(\dot{\omega} \times \hat{\mathbf{r}}\right) \cdot \hat{\mathbf{r}} = 0 \qquad \text{(A9)}$$

as the vector product of two vectors is perpendicular to each of the two vectors. We have proved the specific result that the northward component of a rigid body rotation is invariant in the north-south direction. The proof can be easily generalized to any great circle by replacing **n** by **t**, a vector pointing along the great circle, and φ by α, an angle measured along the great circle. The relationships between the derivatives of the unit vectors with respect to α and the unit vectors themselves are similar to those above.

[53] **Acknowledgments.** We thank R. Reilinger, R. King, and W. Thatcher for their reviews that helped to improve the manuscript. We also thank the Editors for their suggestions. The work presented here benefited from fruitful discussion with J. Jackson. We are grateful to Semih Ergintav and his coworkers for providing us a preprint version of their manuscript, which helped us to assess the effect of the postseismic deformation following the Izmit-Düzce 1999 earthquakes. Finally, we are in debt to A. Ihsan Kurt whose work has been crucial at the beginning of this work. This work was supported by the Natural Environmental Research Council through a grant to the Centre for the Observation and Modelling of Earthquakes and Tectonics (COMET).

References

Altamimi, Z., P. Sillard, and C. Boucher (2002), ITRF2000: A new release of the International Terrestrial Reference Frame for earth science applications, *J. Geophys. Res.*, *107*(B10), 2214, doi:10.1029/2001JB000561.

Altamimi, Z., X. Collilieux, J. Legrand, B. Garayt, and C. Boucher (2007), ITRF2005: A new release of the International Terrestrial Reference Frame based on time series of station positions and Earth Orientation Parameters, *J. Geophys. Res.*, *112*, B09401, doi:10.1029/2007JB004949.

Ambraseys, N. N., and J. A. Jackson (1998), Faulting associated with historical and recent earthquakes in the Eastern Mediterranean region, *Geophys. J. Int.*, *133*, 390–406, doi:10.1046/j.1365-246X.1998.00508.x.

Angelier, J., J. F. Dumont, H. Karamenderesi, A. Poisson, S. Simsek, and S. Uysal (1981), Analysis of fault mechanisms and expansion of southwestern Anatolia since the late Miocene, *Tectonophysics*, *75*, T1–T9, doi:10.1016/0040-1951(81)90271-7.

Blewitt, G., and D. Lavalle (2002), Effect of annual signals on geodetic velocity, *J. Geophys. Res.*, *107*(B7), 2145, doi:10.1029/2001JB000570.

Briole, P., A. Rigo, H. Lyon-Caen, J. C. Ruegg, K. Papazissi, C. Mitsakaki, A. Balodimou, G. Veis, D. Hatzfeld, and A. Deschamps (2000), Active deformation of the Corinth rift, Greece: Results from repeated Global Positioning System surveys between 1990 and 1995 (2006), *J. Geophys. Res.*, *105*(B11), 25,605–25,626, doi:10.1029/2000JB900148.

Brockmann, E. (1996), Combination of solutions for geodetic and geodynamic applications of the Global Positioning System (GPS), Ph.D. dissertation, Astron. Inst., Univ. of Berne, Berne, Switzerland.

Clarke, P. J., et al. (1998), Crustal strain in central Greece from repeated GPS measurements in the interval 1989–1997, *Geophys. J. Int.*, *135*, 195–214, doi:10.1046/j.1365-246X.1998.00633.x.

Dewey, J. F., and A. M. C. Sengor (1979), Aegean and surrounding regions: complex multiplate and continuum tectonics in a convergent zone, *Geol. Soc. Am. Bull.*, *90*, 84–92, doi:10.1130/0016-7606(1979)90<84:AASRCM>2.0.CO;2.

Dong, D., T. A. Herring, and R. W. King (1998), Estimating regional deformation from a combination of space and terrestrial data, *J. Geod.*, *72*, 200–211, doi:10.1007/s001900050161.

Dong, D., P. Fang, Y. Bock, M. K. Cheng, and S. Miyazaki (2002), Anatomy of apparent seasonal variations from GPS-derived site position time series, *J. Geophys. Res.*, *107*(B4), 2075, doi:10.1029/2001JB000573.

Eanes, R. J., and A. Schuler (1999), An improved global ocean tide model from TOPEX/POSEIDON altimetry: CSR4.O, paper presented at EGS 24th General Assembly, The Hague, Netherlands.

Ergintav, S., R. Burgmann, S. McClusky, R. Cakmak, R. E. Reilinger, O. Lenk, A. Barka, and H. Ozener (2002), Postseismic deformation near the Izmit earthquake (17 August 1999, M 7.5) rupture zone, *Bull. Seismol. Soc. Am.*, *92*(1), 194–207, doi:10.1785/0120000836.

Ergintav, S., S. McClusky, E. Hearn, R. Reilinger, R. Cakmak, T. Herring, H. Ozener, O. Lenk, and E. Tari (2009), Seven years of postseismic deformation following the 1999, M = 7.4 and M = 7.2, Izmit-Düzce, Turkey earthquake sequence, *J. Geophys. Res.*, *114*, B07403, doi:10.1029/2008JB006021.

Eyidogan, H., and J. Jackson (1985), A seismological study of normal faulting in the Demirci, Alaehir and Gediz earthquakes of 1969–70 in western Turkey: implications for the nature and geometry of deformation in the continental crust, *Geophys. J. Int.*, *81*(3), 569–607, doi:10.1111/j.1365-246X.1985.tb06423.x.

Goldsworthy, M., and J. Jackson (2000), Active normal fault evolution in Greece revealed by geomorphology and drainage patterns, *J. Geol. Soc.*, *157*, 967–981.

Herring, T. A., J. L. Davis, and I. I. Shapiro (1990), Geodesy by radio interferometry: The application of Kalman filtering to the analysis of very long baseline interferometry data, *J. Geophys. Res.*, *95*, 12,561–12,581, doi:10.1029/JB095iB08p12561.

Herring, T. A., R. W. King, and S. C. McClusky (2006), GLOBK Reference Manual: Global Kalman filter VLBI and GPS analysis program, release 10.3, Dep. of Earth, Atmos., and Planet. Sci., Mass. Inst. of Technol., Cambridge.

Jackson, J. A., and D. McKenzie (1988), The relationship between plate motions and seismic moment tensors, and the rates of active deformation in the Mediterranean and Middle East, *Geophys. J. Int.*, *93*, 45–73, doi:10.1111/j.1365-246X.1988.tb01387.x.

King, R., and Y. Bock (2006), Documentation for the GAMIT GPS analysis software, version 10.3, Mass. Inst. of Technol., Cambridge.

Le Pichon, X. (1982), Land-locked oceanic basins and continental collision: The eastern Mediterranean as a case example, in *Mountain Building Processes*, edited by K. Hsü, pp. 129–146, Academic, London.

McCarthy, D., and G. Petit (Eds.) (2004), IERS Conventions (2003), *IERS Tech. Note 32*, 127 pp., Verl. des Bundesamts fur Kartogr. und Geod, Frankfurt am Main, Germany.

McClusky, S., et al. (2000), Global Positioning System constraints on plate kinematics and dynamics in the eastern Mediterranean and Caucasus, *J. Geophys. Res.*, *105*(B3), 5695–5720, doi:10.1029/1999JB900351.

McKenzie, D. (1972), Active tectonics of the Mediterranean region, *Geophys. J. R. Astron. Soc.*, *30*, 109–185.

Meade, B. J., B. H. Hager, S. C. McClusky, R. E. Reilinger, S. Ergintav, O. Lenk, A. Barka, and H. Ozener (2002), Estimates of seismic potential in the Marmara region from block models of secular deformation constrained by GPS measurements, *Bull. Seismol. Soc. Am.*, *92*, 208–215, doi:10.1785/0120000837.

Nocquet, J.-M., E. Calais, Z. Altamimi, P. Sillard, and C. Boucher (2001), Intraplate deformation in western Europe deduced from an analysis of the International Terrestrial Reference Frame 1997 (ITRF97) velocity field, *J. Geophys. Res.*, *106*(B6), 11,239–11,257, doi:10.1029/2000JB900410.

Nyst, M., and W. Thatcher (2004), New constraints on the active tectonic deformation of the Aegean, *J. Geophys. Res.*, *109*, B11406, doi:10.1029/2003JB002830.

Okada, Y. (1985), Surface deformation due shear and tensile faults in a half-space, *Bull. Seismol. Soc. Am.*, *75*, 1135–1154.

Reilinger, R., et al. (2006), GPS constraints on continental deformation in the Africa-Arabia-Eurasia continental collision zone and implications for the dynamics of plate interactions, *J. Geophys. Res.*, *111*, B05411, doi:10.1029/2005JB004051.

Rothacher, M., and L. Mervart (1996), The Bernese GPS software version 4.0, Astron. Inst., Univ. of Berne, Berne, Switzerland.

Saroglu, F., O. Emre, I. Kuscu, A. Boray, A. Barka, S. Ozer, and S. Sirin (1992), Active fault map of Turkey, Gen. Dir. of Miner. Res. and Explor., Ankara, Turkey.

Saunders, P., K. Priestley, and T. Taymaz (1998), Variations in the crustal structure beneath western Turkey, *Geophys. J. Int.*, *134*, 373–389, doi:10.1046/j.1365-246x.1998.00571.x.

Savage, J. C. (1983), A dislocation model of strain accumulation and release at a subduction zone, *J. Geophys. Res.*, *88*, 4984–4996, doi:10.1029/JB088iB06p04984.

Sodoudi, F., R. Kind, D. Hatzfeld, K. Priestley, W. Hanka, K. Wylegalla, G. Stavrakakis, A. Vafidis, H.-P. Harjes, and M. Bohnhoff (2006), Lithospheric structure of the Aegean obtained from P and S receiver functions, *J. Geophys. Res.*, *111*, B12307, doi:10.1029/2005JB003932.

ten Veen, J. H., J. M. Woodside, T. A. C. Zitter, J. F. Dumont, J. Mascle, and A. Volkonsaia (2004), Neotectonic evolution of the Anaximander Mountains at the junction of the Hellenic and Cyprus arcs, *Tectonophysics*, *391*, 35–65, doi:10.1016/j.tecto.2004.07.007.

Van Dam, T., J. Wahr, P. C. D. Milly, A. B. Shmakin, G. Blewitt, D. Lavallee, and K. M. Larson (2001), Crustal displacements due to continental water loading, *Geophys. Res. Lett.*, *28*, 651–654, doi:10.1029/2000GL012120.

Williams, S. D. P. (2003), The effect of coloured noise on the uncertainties of rates estimated from geodetic time series, *J. Geod.*, *76*(9–10), 483–494, doi:10.1007/s00190-002-0283-4.

Williams, S. D. P., Y. Bock, P. Fang, P. Jamason, R. M. Nikolaidis, L. Prawirodirdjo, M. Miller, and D. J. Johnson (2004), Error analysis of

continuous GPS position time series, *J. Geophys. Res.*, *109*, B03412, doi:10.1029/2003JB002741.

H. Akdeniz, B. Aktug, A. Cingöz, Y. Erkan, M. A. Gürdal, A. Kilicoglu, O. Lenk, and A. Tekgül, General Command of Mapping, Tip Fakultesi Caddesi, 06100 Cebeci, Ankara, Turkey. (bahadir.aktug@hgk.mil.tr; ayhan.cingoz@hgk.mil.tr; yasin.erkan@hgk.mil.tr; mehmetali.gurdal@hgk.mil.tr; ali.kilicoglu@hgk.mil.tr; onur.lenk@hgk.mil.tr; ayhan.tekgul@hgk.mil.tr)

P. England and B. Parsons, COMET, Department of Earth Sciences, Parks Road, Oxford OX1 3PR, UK. (Philip.England@earth.ox.ac.uk; barry.parsons@earth.ox.ac.uk)

J. M. Nocquet, Geosciences Azur, University of Nice-Sophia-Antipolis, CNRS, F-06560 Valbonne, France. (nocquet@geoazur.unice.fr)